

A Godunov–type scheme for a scalar conservation law with space-time flux discontinuity

Kwame Atta Gyamfi^{1,2*†}

¹ Istituto Nazionale di Geofisica e Vulcanologia, Roma1, L’Aquila, Italy.

²Department of Mathematics, Kwame Nkrumah University of Science and
Technology, Kumasi, Ghana.

Corresponding author(s). E-mail(s): kwame.gyamfi@ingv.it;

[†]**Acknowledgments:** The author acknowledges the support and guidance of Prof. Debora Amadori during their doctoral studies at the University of L’Aquila. Additionally, the author expresses gratitude to the research group of Prof. Carlotta Donadello at the University of Franche-Comté Besançon for their hospitality during research visits.

Abstract

We present and analyze a new finite volume scheme of Godunov-type for a nonlinear scalar conservation law whose flux function has a discontinuous coefficient due to time-dependent changes in its sign along a Lipschitz continuous curve.

Keywords: finite volume scheme, scalar conservation laws, discontinuous flux, moving interface, numerical analysis, moving mesh

MSC Classification: 65M08 , 65M50 , 65M22 , 35A35 , 35L65 , 35L60

1 Introduction

In this article, we propose a numerical scheme for solving a scalar conservation law with a flux function that is discontinuous in space and time. The equation writes

$$\begin{cases} \partial_t \rho + \partial_x F(t, x, \rho) = 0, \\ \rho(0, x) = \rho_0(x), \quad \rho(t, \pm 1) = 0, \end{cases} \quad (1.1)$$

in which

- $t \in \mathbb{R}^+ = [0, \infty)$ is the time variable and $x \in \Omega =] - 1, 1[$ is the space variable;
- $(t, x) \mapsto \rho(t, x)$ is the unknown function, and $\rho \in \mathbf{L}^\infty(\mathbb{R}^+ \times \Omega; [0, 1])$;
- F representing the flux function is given by

$$F(t, x, \rho) \doteq \text{sign}(x - \xi(t))f(\rho) \quad (1.2)$$

where

$$f : [0, 1] \rightarrow \mathbb{R}^+ \text{ is concave, } f(0) = 0 = f(1), \quad \max_{\rho \in [0, 1]} f(\rho) > 0, \quad \lim_{\rho \rightarrow 0^+} \frac{f(\rho)}{\rho} \in \mathbb{R}; \quad (1.3)$$

$$\xi : \mathbb{R}^+ \rightarrow \Omega \text{ is Lipschitz continuous with } \left[\inf_{\mathbb{R}^+} \xi, \sup_{\mathbb{R}^+} \xi \right] \subset (-1, 1). \quad (1.4)$$

As equation (1.1) is a fundamental law, most partial differential equations (PDEs) problems arising in the physical and engineering sciences can be formulated in its form. Examples can be found in (1) porous media: modeling the two-phase flow in porous media [25, 28] and continuous sedimentation in ideal clarifier-thickener units [13]; (2) traffic flow: modeling a toll gate along a highway [16] and traffic flow with changing road surface conditions [12, 34]; (3) ion etching in semiconductor device fabrication [35]; (4) pedestrian flow models [27, 4, 32].

More precisely, equation (1.1) derives from the one-dimensional Hughes model [27] of pedestrian flow in a narrow corridor with fixed exits at $x = \pm 1$. However, in contrast to the Hughes model, the time-dependent flux interface $\xi(t)$ considered in this work is not required to satisfy the implicit relation involving a monotone cost function $c(\rho)$

$$\int_{-1}^{\xi(t)} c(\rho(t, x)) dx = \int_{\xi(t)}^1 c(\rho(t, x)) dx, \quad \forall t \geq 0. \quad (1.5)$$

Therefore, the equation considered in this work assumes no nonlocal conditions on the flux via the turning curve $x = \xi(t)$ even though the numerical scheme proposed here can easily be adapted to solve Hughes' model. It is worth noting that in the context of this model, the function $\xi(t)$ is commonly known as the turning curve and represents the points where pedestrians change direction to optimize the distance or time required to reach exits. See [4]. In this paper, we will use the term "flux interface" or simply "the interface" to refer to ξ . Moreover, we will refer to a scalar conservation law with discontinuous flux as the discontinuous flux problem.

Research works dedicated to solutions to discontinuous flux problems have been extensively documented in the literature. See articles [28, 1, 21, 37, 10, 30, 8, 19, 2, 6, 38, 10]. It is a well-known fact that even if the flux function is continuous and the initial data do not contain jump discontinuities, the global Cauchy problem for a scalar conservation law does not admit classical solutions that are valid for all times $t > 0$. Thus, there exists a finite time beyond which classical solutions develop discontinuities, such as shock waves. The occurrence of these irregularities in the solution, which is severe for equations with discontinuous coefficients such as (1.1), is largely attributed to the nonlinearity of the flux function. For example, equation (1.1) generalizes to the system

$$\partial_t \rho + \partial_x (k(t, x)f(\rho)) = 0, \quad k_t = 0 \quad (1.6)$$

whose speed matrix (or Jacobian matrix) after writing (1.6) in nonconservative form has a repeated zero eigenvalue for some values of (ρ, k) . For this reason, the appropriate setting for an admissible solution is the space of discontinuous functions, such as the space of \mathbf{L}^∞ functions, in which a shock wave is well-defined. Such solutions are sought in the weak (or distributional) sense and hence are referred to as weak solutions [22]. Popular methods to construct solutions include numerical approximation methods based on finite volume/difference schemes [9, 13, 29, 31], wavefront tracking algorithm [26, 25, 15], and others. In this paper, we discuss the existence of entropy weak solution to (1.1) by constructing the approximate solution via a finite volume method exclusive to this class of equations.

In general, deriving an existence theory for a class of hyperbolic conservation law relies on *a priori* estimates with which a compactness argument can be used 'to pass to the limit' in the solution through an appropriate compactness theory such as Helly's theory. However, for selected time-dependent discontinuous flux problems, such as (1.1), such estimates are difficult to obtain or nonexistent, even after transforming approximate solutions via an appropriate singular mapping, as was done in [15]. In such situations, alternative approaches that are free from these estimates, including compensated compactness (see [29]), measure-valued solutions (see [7]), and kinetic formulation (see [20]), provide handy tools to establish rigorous existence results. In the latter two cases, it is enough to use only standard estimates, such as the so-called "weak BV estimates," to prove the convergence of the approximate solution to the entropy process solution under appropriate CFL conditions [24, 23].

The notion of entropy solutions for discontinuous flux problems does not follow the standard notions suitable for a generic conservation law with continuous coefficients. The main ideas of entropy solutions for discontinuous flux problems rely on applying Kruzhkov's admissibility conditions away from the flux interface but enforcing additional "entropy conditions" at the interface to aid the selection of unique and admissible solutions. It has been argued in [2] that as a result of this occurrence, there exists an infinite number of L^1 contractive semigroups, each associated with an interface connection, for a variety of discontinuous flux problems. The principal features of entropy solutions are the shape of the flux and the traces in the solution at the interface (i.e., the so-called $A - B$ entropy connection) [5, 21, 6]. In the work of [8], these concepts were unified by the introduction of a new framework called admissibility germs \mathcal{G} (or "germs" for short) within which the entropy solutions described above reduced to elementary solutions of piecewise constant nature provided their traces satisfy a form of a Rankine-Hugoniot condition at the interface. In our context, this family of piecewise constant constant solutions, typically described by ordered pairs (p_l, p_r) of the form $p_l \chi_{x < \xi(t)} + p_r \chi_{x > \xi(t)}$, with p_l and p_r in $[0, R]$ are maximal and complete.

In this context, we present and analyze a finite volume scheme to solve a scalar conservation law with a single time-dependent flux discontinuity that switches the sign of the flux coefficient between $+1$ and -1 at each $t > 0$. We deal with the discontinuity by introducing a moving mesh near ξ in the discrete space-time domain and then adapt the value of the flux there based on the slope $\dot{\xi}$. Standard finite volume schemes for continuous flux problems involve discretizing the space domain into numerical cells bounded by grid points. Then the solution for each discrete time is approximated by solving a 'local' Riemann problem at each grid point whose results are unionized to obtain the solution at the next time step. Here, the moving mesh consists in removing grid points nearest to ξ so that the CFL condition is not violated. This approach introduced by [39], has been used to study traffic flow models on a highway with a mobile bottleneck [17,

[14, 18]. Indeed, the scheme proposed in these works was only analyzed in a mathematically rigorous in [36] where existence and uniqueness results were obtained in a fashion similar to ours. However, the scheme of [36] uses the Engquist-Osher flux on standard mesh away from the moving interface and the Godunov numerical fluxes at the interfaces with the moving mesh and a flux crossing condition. This scheme was later extended in [9], where the existence of solutions for conservation laws with multiple space-time flux interface discontinuities. Indeed, any standard 'entropy' numerical flux such as the Godunovs, Lax-Friedrich's, etc, works well for treating solutions away from the interfaces as long as it is monotone and consistent. We would like to highlight that the analysis conducted in [9] bears similarity to our own, and it may be considered more comprehensive, as it accounts for multiple moving interfaces. Nevertheless, considering the scarcity of contributions addressing space-time discontinuous flux problems, our work serves as an additional and valuable contribution to this field.

The remainder of the paper is organized into four main sections. Section 2 focuses on the theoretical aspect of the problem and discusses the Riemann problem for (1.1), including the Riemann solver at ξ . Here, we present the framework of admissibility germs and prove the relevant properties that could later be extended to obtain a comprehensive theory of the existence of weak entropy solutions in the next article. The next section, Section 3, presents the numerical scheme and the mesh adaptations (the moving mesh), detailing all possible cases due to changes in slope of ξ . Furthermore, approximate entropy inequalities and a uniform \mathbf{L}^∞ bound on the numerical approximations are also presented. Finally, in Section 5, we furnish details about the chosen examples, present their numerical simulations, and use them to explore the numerical convergence of the scheme achieved by calculating the error \mathbf{L}^1 , which is provided for each example.

2 Problem setting

We start this section by defining a weak entropy solution of (1.1), which will be featured throughout the paper.

Definition 2.1. *Assume that f, ξ satisfy (1.3), (1.4), respectively. We say that map $(t, x) \mapsto \rho(t, x)$ is a weak entropy solution to the initial-boundary value problem (1.1), if ρ is in $\mathbf{C}^0([0, +\infty[; \mathbf{L}^\infty(\Omega; [0, 1]))$ and for any $c \in [0, 1]$, and any test function $\varphi \in \mathbf{C}_c^\infty(\mathbb{R}^2; [0, +\infty[)$, the following Kružkhov-type entropy inequality holds:*

$$\begin{aligned} & \int_0^{+\infty} \int_{-1}^1 [|\rho - c| \partial_t \varphi + \mathcal{F}(t, x, \rho, c) \partial_x \varphi] dx dt + \int_{-1}^1 |\rho_0(x) - c| \varphi(0, x) dx \\ & + \int_0^{+\infty} [f(\rho(t, 1-)) - f(c)] \varphi(t, 1) dt + \int_0^{+\infty} [f(\rho(t, -1+)) - f(c)] \varphi(t, -1) dt \\ & + 2 \int_0^{+\infty} f(c) \varphi(t, \xi(t)) dt \geq 0, \end{aligned} \quad (2.7)$$

where, recalling (1.2),

$$\begin{aligned} \mathcal{F}(t, x, \rho, c) & \doteq \text{sign}(\rho - c) [F(t, x, \rho) - F(t, x, c)] \\ & = \text{sign}(\rho - c) \text{sign}(x - \xi(t)) [f(\rho) - f(c)]. \end{aligned} \quad (2.8)$$

The first line in (2.7) originates from the Kruřkov definition of entropy weak solution as would be in the case of a Cauchy problem, [33]. The two terms in the second line come from the boundary condition introduced by Bardos et al. in [11] whereas the term in the last line accounts for the traces in the solution along the discontinuity in the flux.

2.1 The Riemann problem at turning curve

The solution of the Riemann problem serves as building block for the selection of a numerical scheme appropriate for the equation under consideration. Since our equation contains a jump at the flux interface, it is necessary to construct a Riemann solver at the interface. In this section, we present the Riemann solver for (1.1) and detail the types of admissible elementary waves that are present in solution at $\xi(t)$.

Let $\xi(t) = \alpha t$ with $\alpha \in \mathbb{R}$, and consider the Riemann problem

$$\partial_t \rho + \partial_x (\text{sign}(x - \alpha t) f(\rho)) = 0, \quad x \in \mathbb{R}, \quad t > 0 \quad (2.9)$$

$$\rho_0(x) = \begin{cases} \rho_L, & \text{if } x < 0, \\ \rho_R, & \text{if } x > 0 \end{cases} \quad (2.10)$$

with $\rho_L, \rho_R \in [0, 1]$. We look for a self-similar solution of the problem (2.9), (2.10) according to the Definition 2.1, that we will denote by $\mathcal{R}^\alpha(\rho_L, \rho_R)(t, x)$.

Also, we will denote by $\mathcal{R}^\pm(\rho_L, \rho_R)(t, x)$ the classical Riemann solver for

$$\partial_t \rho \pm \partial_x f(\rho) = 0, \quad x \in \mathbb{R}, \quad t > 0$$

with initial data (2.10) at $t = 0$.

Let's define

$$v(\rho) \doteq \begin{cases} \frac{f(\rho)}{\rho}, & \rho \in (0, R] \\ \lim_{\rho \rightarrow 0^+} \frac{f(\rho)}{\rho} & \rho = 0. \end{cases}$$

After the assumption (1.3) on f , the function $v(\rho)$ is non-increasing and $v(0)$ is well defined and finite.

In practice, we can distinguish between two cases: either $\alpha \in [-v(\rho_L), v(\rho_R)]$ or not.

- $-v(\rho_L) \leq \alpha \leq v(\rho_R)$ In this case, for any couple $(\rho_L, \rho_R) \in [0, 1]^2$, the function

$$\mathcal{R}^\alpha(\rho_L, \rho_R)(t, x) = \begin{cases} \mathcal{R}^-(\rho_L, 0)(t, x), & \text{for } x < 0, \\ \mathcal{R}^+(0, \rho_R)(t, x), & \text{for } x > 0. \end{cases} \quad (2.11)$$

is a solution to (2.9), (2.10) in the sense of Definition 2.1.

More precisely, the solution takes the form

$$\mathcal{R}^\alpha(\rho_L, \rho_R)(t, x) = \begin{cases} \rho_L, & \text{for } x < -v(\rho_L)t, \\ 0, & \text{for } x/t \in (-v(\rho_L), v(\rho_R)), \\ \rho_R, & \text{for } x > v(\rho_R)t, \end{cases} \quad (2.12)$$

because the waves joining ρ_L to 0 and 0 to ρ_R , with flux $-f$ and f respectively, are necessarily shock discontinuities. See Figure 1.

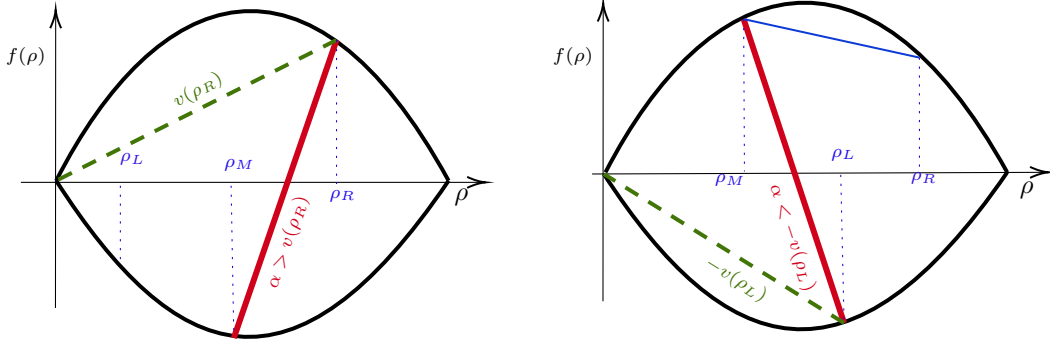


Fig. 1 The Riemann solvers at turning curve for the initial data (2.10), with $\alpha > v(\rho_R)$ (left) and $\alpha < -v(\rho_L)$ (right).

- $\alpha \geq v(\rho_R)$ For this case we have

$$\mathcal{R}^\alpha(\rho_L, \rho_R)(t, x) = \begin{cases} \mathcal{R}^-(\rho_L, \rho_M)(t, x), & \text{for } x < \alpha t, \\ \rho_R, & \text{for } x > \alpha t, \end{cases} \quad (2.13)$$

where ρ_M is the only density value in $[0, \rho_R)$ such that the jump condition across $\xi(t) = \alpha t$,

$$\alpha = \frac{f(\rho_R) + f(\rho_M)}{\rho_R - \rho_M}. \quad (2.14)$$

is satisfied.

- $\alpha < -v(\rho_L)$ On the other hand, if $\alpha < -v(\rho_L)$, the Riemann solver is similarly written

$$\mathcal{R}^\alpha(\rho_L, \rho_R)(t, x) = \begin{cases} \rho_L, & \text{for } x < \alpha t, \\ \mathcal{R}^+(\rho_M, \rho_R)(t, x), & \text{for } x > \alpha t, \end{cases} \quad (2.15)$$

where the intermediate state value $\rho_M \in [0, \rho_L)$ satisfies

$$\alpha = \frac{f(\rho_M) + f(\rho_L)}{\rho_M - \rho_L}. \quad (2.16)$$

See Figure 1 above. The following lemma shows that the intermediate state value is unique.

Lemma 2.2. *Let f satisfy (1.3). Then for any given $\rho_R \in (0, 1)$ and $\alpha > v(\rho_R)$ there exists a unique $\rho_M \in (0, \rho_R)$ which satisfies (2.14).*

Proof. Define the map

$$\Phi(\rho) = \frac{f(\rho_R) + f(\rho)}{\rho_R - \rho}, \quad \rho \in (0, \rho_R).$$

It is immediate to see that

$$\lim_{\rho \rightarrow 0^+} \Phi(\rho) = f(\rho_R)/\rho_R = v(\rho_R), \quad \lim_{\rho \rightarrow \rho_R^-} \Phi(\rho) = +\infty, \quad (2.17)$$

and, by convexity of f , we have that

$$\Phi'(\rho) = \frac{f'(\rho)(\rho_R - \rho) + f(\rho_R) + f(\rho)}{(\rho_R - \rho)^2} \geq \frac{2f(\rho_R)}{(\rho_R - \rho)^2} > 0. \quad (2.18)$$

Therefore Φ is strictly increasing, and there exists a unique solution to (2.14). This completes the proof of the lemma. \square

To ensure that the Riemann solver in (2.13) is well defined, a necessary condition is that for any couple (ρ_L, ρ_R) and $\alpha > f(\rho_R)/\rho_R$ the speed of waves in $\mathcal{R}^-(\rho_L, \rho_M)$ is lower than α . This condition is easily verified, thanks to the convexity of $-f$.

Proposition 2.1. *The following bounds hold for all $\alpha \in \mathbb{R}$,*

$$0 \leq \mathcal{R}^\alpha(\rho_L, \rho_R)(x/t) \leq \max\{\rho_L, \rho_R\}. \quad (2.19)$$

Remark 1. *Since the flux switches sign, the solution to the Riemann problem satisfies the equation with convex flux $-f(\rho)$ on the domain $\Omega_L = \{(x, t) : x < \alpha t\}$, and with concave flux $+f(\rho)$ on $\Omega_R = \{(x, t) : x > \alpha t\}$.*

Suppose the pair $(\gamma_l \rho(t), \gamma_r \rho(t))$ are the left and right traces at $\xi(t)$ at each $t > 0$, then definition 2.1 yields the Rankine-Hugoniot condition

$$f(\gamma_r \rho(t)) + f(\gamma_l \rho(t)) = \xi'(t)(\gamma_r \rho(t) - \gamma_l \rho(t)), \quad (2.20)$$

at $\xi(t)$.

As a consequence of Definition 2.1, if the solution is discontinuous at $x = \xi(t)$ the jump is undercompressive and the characteristic lines impinge on $\xi(t)$ from the side where the density is higher. More precisely, if ρ is an entropy solution and $(\gamma_l \rho(t), \gamma_r \rho(t))$ are its left and right traces at $\xi(t)$, at each $t > 0$ we have

$$\min\{0, -\xi'(t) - f'(\gamma_l \rho(t))\} \max\{0, -\xi'(t) + f'(\gamma_r \rho(t))\} = 0. \quad (2.21)$$

This necessary condition has been pointed out in [30, Prop. 5.1] in a more general framework and in [32, Prop. 2.4] for the Hughes model. The numerical examples used in Section 5 well illustrates this effect.

2.2 The germ of admissible solutions

The time-dependent discontinuity of f in ρ along the Lipschitz continuous curve ξ makes it more appropriate to consider entropy solutions given in Definition (2.1) within the admissibility germ

framework. In this framework, the inequality (2.7) reduces to a pair of traces at ξ if the condition (2.20) is satisfied. It is important to note that since $\pm f$ are assumed to be continuous over $[0, R]^2$ and the measure of the set $\{s \in [0, 1] \text{ s.t. } f'(s) = 0\}$ is zero, the traces $\gamma^{l,r} \rho(t)$ are actually one-sided strong traces, as proven in [8, Theorem 2.1]. This notion of admissibility germs relies on the idea that Kruzhkov's entropy is satisfied away from ξ , while the "non-standard" Rankine-Hugoniot condition is adapted at ξ . Thanks to the germs, it should be possible to define the notion of an entropy process solution. We proceed to define the germ below.

Definition 2.3. Let $\xi(t) = \alpha t$, with $\alpha \in \mathbb{R}$ fixed. The germ of admissible solutions \mathcal{G}_α for the conservation law (1.1) is

$$\mathcal{G}_\alpha := \{(0, \rho_\alpha) \in [0, 1]^2 : f(\rho_\alpha) = \alpha \rho_\alpha\}. \quad (2.22)$$

Definition 2.4. A germ \mathcal{G} is L^1 -dissipative (L^1D for short), if for any $(p_l, p_r), (q_l, q_r) \in \mathcal{G}(\xi)$ the following dissipative property holds

$$\mathcal{F}(t, x, p_l, q_l) - \mathcal{F}(t, x, p_r, q_r) \geq \alpha(\eta(p_l, q_l) - \eta(p_r, q_r)), \quad (2.23)$$

where $\mathcal{F}(t, x, \rho, c)$ is defined in Definition (2.1) and $\eta(\rho, c) := |\rho - c|$.

Proposition 2.2. The unique maximal L^1D extension of \mathcal{G}_α is the subset of $[0, 1]^2$ defined by

$$\tilde{\mathcal{G}}_\alpha := \{(p_l, p_r) \in [0, 1]^2 : f(p_r) + f(p_l) = \alpha(p_r - p_l)\}. \quad (2.24)$$

Proof. The fact that $\tilde{\mathcal{G}}_\alpha$ contains \mathcal{G}_α is obvious as

$$f(\rho_\alpha) + f(0) = \alpha \rho_\alpha - 0.$$

To show that $\tilde{\mathcal{G}}_\alpha$ is L^1D we distinguish three cases : $\alpha = 0$, $\alpha > 0$, and $\alpha < 0$.

If $\alpha = 0$ the germ only contains four elements $(0, 0)$, $(0, 1)$, $(1, 0)$, $(1, 1)$ and we can check that (2.23) holds as an equality by direct computations.

If $\alpha > 0$ we consider two sub-cases

I. If $q_l = q_r = 0$ we have

$$\begin{aligned} \mathcal{F}(t, x, p_l, 0) - \mathcal{F}(t, x, p_r, 0) &= (-f(p_l) + f(0)) - (f(p_r) - f(0)) \\ &= -(f(p_r) + f(p_l)) = \alpha(p_l - q_r) \\ &= \alpha(\eta(p_l, 0) - \eta(p_r, 0)), \end{aligned}$$

for all $p_l, p_r \in [0, 1]^2$. The case in which $q_l = q_r = 1$ is similar.

II. If $q_l < q_r$ (the reverse inequality being impossible due to the sign of α and the geometry of the problem) we can observe that

$$\text{sign}(p_l - q_l) = \text{sign}(p_r - q_r).$$

Therefore

$$\begin{aligned}
\mathcal{F}(t, x, p_l, q_l) - \mathcal{F}(t, x, p_r, q_r) &= \text{sign}(p_l - q_l) (-f(p_l) + f(q_l) - f(p_r) + f(q_r)) \\
&= \text{sign}(p_l - q_l) \alpha (q_r - q_l - p_r + p_l) \\
&= \alpha (\eta(p_l, q_l) - \eta(p_r, q_r)).
\end{aligned}$$

If $\alpha < 0$ the analysis is exactly the same as in the previous case.

It is also clear that $\tilde{\mathcal{G}}_\alpha$ is maximal: given any L^1D germ \mathcal{G} one can look for its possible L^1D extensions, the largest of which is its dual \mathcal{G}^* , i.e. the set containing all couples $(q_l, q_r) \in [0, R]^2$ which satisfy the Rankine-Hugoniot conditions and (2.23) for any $(p_l, p_r) \in \mathcal{G}$. Of course, $\tilde{\mathcal{G}}_\alpha$ and $\tilde{\mathcal{G}}_\alpha^*$ coincide. \square

Additionally, given any piecewise constant initial condition $\rho_l \chi_{x < \xi(t)} + \rho_r \chi_{x > \xi(t)}$, with ρ_l and $\rho_r \in [0, 1]$, then the left and right side traces of the solution of the associate Riemann problem correspond to an element of $\tilde{\mathcal{G}}_\alpha$. More formally

Lemma 2.5. *For any $\xi = \alpha t$, the L^1D germ $\tilde{\mathcal{G}}_\alpha$ is complete.*

Proof. This lemma follows immediately from the study of the Riemann problem at the interface in 2.1. \square

We now define \mathcal{G} -entropy and \mathcal{G} -entropy process solutions for our problem below.

Definition 2.6. *Assume that f, ξ satisfy (1.3), (1.4) respectively. We say that map $(t, x) \mapsto \rho(t, x)$ is a \mathcal{G} -entropy solution to the initial-boundary value problem (1.1), if ρ in $\mathbf{L}^\infty([0, +\infty[\times \Omega; [0, 1])$, is a weak solution of this problem and for any $(p_l, p_r) \in \mathcal{G}$, and any test function $\varphi \in \mathbf{C}_c^\infty(\mathbb{R}^2; [0, +\infty[)$ we have*

$$\begin{aligned}
& \int_0^{+\infty} \int_{-1}^1 [|\rho - c(x)| \partial_t \varphi + \mathcal{F}(t, x, \rho, c(x)) \partial_x \varphi] dx dt + \int_{-1}^1 |\rho_0(x) - c(x)| \varphi(0, x) dx \\
& + \int_0^{+\infty} [f(\rho(t, 1-)) - f(c(x))] \varphi(t, 1) dt + \\
& + \int_0^{+\infty} [f(\rho(t, -1+)) - f(c(x))] \varphi(t, -1) dt \geq 0,
\end{aligned} \tag{2.25}$$

where $c(x) = p_l \chi_{x < \xi(t)}(x) + p_r \chi_{x > \xi(t)}(x)$ and $\mathcal{F}(t, x, \rho, c)$ is defined at (2.8).

Remark 2. *Following [8, Remark 3.12 and Th. 3.18] we recall that*

- $\rho \in \mathbf{L}^\infty([0, +\infty[\times \Omega; [0, 1])$ is a \mathcal{G}_α -entropy solution if and only if it is an entropy solution in the sense of Kruzhkov on $[0, +\infty[\times [-1, \xi^-]$ and $[0, +\infty[\times (\xi^+, 1]$, and for almost every $t > 0$ the couple given by its traces at $x = \xi(t)$, $(\gamma^l \rho(t), \gamma^r \rho(t))$, is in $\tilde{\mathcal{G}}_\alpha = \mathcal{G}_\alpha^*$. From the definition of $\tilde{\mathcal{G}}_\alpha$ it is clear that this last point is equivalent to say that ρ is a weak solution on $[0, +\infty[\times \Omega$. Therefore, Definition 2.6 is equivalent to Definition 1 in [3].
- In our setting \mathcal{G}_α - and $\tilde{\mathcal{G}}_\alpha$ -entropy solutions coincide.

Definition 2.7. *Assume that f, ξ satisfy (1.3), (1.4) respectively. We say that a function $\mu \in \mathbf{L}^\infty([0, +\infty[\times \Omega \times (0, 1); [0, 1])$ is a $\tilde{\mathcal{G}}_\alpha$ -entropy process solution to the initial-boundary value problem (1.1), if the following conditions hold :*

1. For any test function $\varphi \in \mathbf{C}_c^\infty(\mathbb{R}^+ \times (-1, 1); [0, +\infty])$ we have

$$\int_0^1 \int_0^{+\infty} \int_{-1}^1 [\mu(t, x, a) \partial_t \varphi + F(t, x, \mu(t, x, a)) \partial_x \varphi] dx dt da + \int_{-1}^1 \rho_0(x) \varphi(0, x) dx = 0,$$

2. The inequality

$$\begin{aligned} & \int_0^1 \int_0^{+\infty} \int_{-1}^1 [|\mu(t, x, a) - c(x)| \partial_t \varphi + \mathcal{F}(t, x, \mu(t, x, a), c(x)) \partial_x \varphi] dx dt da \\ & + \int_{-1}^1 |\rho_0(x) - c(x)| \varphi(0, x) dx \geq 0, \end{aligned} \quad (2.26)$$

where $\mathcal{F}(t, x, \rho, c) = \text{sign}(\rho - c) [F(t, x, \rho) - F(t, x, c)]$, is satisfied

- for any test function $\varphi \in \mathbf{C}_c^\infty(\mathbb{R}^+ \times (-1, 1); [0, +\infty])$ and for any $c(x) = p_l \chi_{x < \xi(t)}(x) + p_r \chi_{x > \xi(t)}(x)$ such that $(p_l, p_r) \in \tilde{\mathcal{G}}_\alpha$;
- for any test function $\varphi \in \mathbf{C}_c^\infty(\mathbb{R}^+ \times (-1, 1); [0, +\infty])$ such that $\varphi = 0$ on $x = \xi(t)$ and any constant $c(x) = c \in \mathbb{R}$.

Remark 3. We could define \mathcal{G}_α -entropy process solutions, but since they do not coincide in general with $\tilde{\mathcal{G}}_\alpha$ -entropy process solutions, we do not use them here. The fact that $\tilde{\mathcal{G}}_\alpha$ is maximal $L^1 D$ is a necessary hypothesis in the following theorem, see [8, Th: 3.28].

Theorem 2.8. Let \mathcal{G} be a maximal $L^1 D$ germ and let ρ_0 be an initial condition for which the initial-boundary value problem (1.1) admits a \mathcal{G} -entropy solution, ρ . Then there exists a unique \mathcal{G} -entropy process solution μ associated to the initial condition ρ_0 and $\mu(\alpha) = \rho$ for almost every $\alpha \in (0, 1)$.

Thanks to the existence result proved in [30] we deduce that our problem admits a unique $\tilde{\mathcal{G}}_\alpha$ -entropy process solution. We will construct this in the next section as the limit of finite volume approximations.

3 The Finite Volume Scheme

In this section, we present a finite volume scheme with a moving mesh adapted near ξ to approximate the weak solution of equation (1.1). Our strategy to define the moving mesh consists in discretizing the space-time domain into a reference mesh, but at each time only cells closer to the flux interface ξ are adapted such that it is included in the computational mesh. The main feature of the computational (or moving) mesh is that the two cells adjacent to ξ have variable lengths, whereas the cells on the reference mesh have a fixed cell length, h . Modified marching formulas, which incorporate a modified numerical flux function based on the non-classical Riemann solver (\mathcal{R}^α), are applied to the two cells adjacent to the turning curve. The standard Godunov marching formulas are used for cells away from ξ , where the reference mesh is established.

This is a slight variation from the mesh adaptation technique presented in [39] and used in [17] for a traffic flow model with a moving constraint. This technique involves replacing the cell interface closest to ξ and shifting the adjacent interfaces, followed by a Lagrange interpolation formula to calculate a new temporal density average for two adjacent cells. Although their scheme is conservative, the recomputation of the new density averages makes it difficult to analyze the

well-balanced property of the resulting scheme. The scheme proposed here does not suffer from this severity. Another variation of the discretization procedure also adapted for the traffic flow model with moving constraints can be found in [36]. In the next subsections, we detail our space discretization procedure and present the numerical scheme.

3.1 Discretization

Fix $N \in \mathbb{N}$ and define $h = 2^{-N}$ as the space step. Let $x_{j+1/2} := (j + 1/2)h$ be a point of the reference mesh and $C_j := [x_{j-1/2}, x_{j+1/2})$ be a computational cell.

Since we are approximating the space interval $\Omega =]-1, 1[$, the indexes $j \in \mathbb{N}$ of the cells are considered in the range $j = -\frac{1}{h}, \dots, \frac{1}{h}$. The leftmost and rightmost cells are

$$C_{-\frac{1}{h}} := \left[x_{-\frac{1}{h}-\frac{1}{2}}, x_{-\frac{1}{h}+\frac{1}{2}} \right), \quad C_{\frac{1}{h}} := \left[x_{\frac{1}{h}-\frac{1}{2}}, x_{\frac{1}{h}+\frac{1}{2}} \right).$$

The computational cells here above contain the boundary points $x = -1$ and $x = 1$ respectively, and

$$\bigcup_{j=-1/h}^{1/h} C_j = \left[-\frac{h}{2} - 1, 1 + \frac{h}{2} \right). \quad (3.27)$$

Let $k > 0$ denote the time step and set $t^n = nk$ for $n \in \mathbb{N}$. We define the slope discretization of $\xi(t)$ as follows,

$$\alpha_{n,k} = \frac{1}{k} \int_{t^n}^{t^{n+1}} \dot{\xi}(t) dt, \quad n \in \mathbb{N} \quad (3.28)$$

and by $\xi^k(t)$ the polygonal function that interpolates linearly the points $(t^n, \xi(t^n))$, that is

$$\xi^k(t^n) = \xi(t^n) =: \xi^n, \quad \frac{d}{dt} \xi^k(t) = \alpha_{n,k} \quad t \in (t^n, t^{n+1}). \quad (3.29)$$

The next definition provides the basic notations and settings for the **moving mesh**.

Definition 3.1. *Let the space step $h = 2^{-N} > 0$ and time step $k > 0$ be fixed. Recalling (1.4), choose $N \geq N_0$ with $N_0 \in \mathbb{N}$ large enough so that $\|\xi\|_\infty < 1 - h/2$ for every $N \geq N_0$. For every $n \in \mathbb{N}$, let $m(n) \in \{-\frac{1}{h} + 1, \dots, \frac{1}{h} - 1\}$ be the single value such that*

$$\xi^n \in [x_{m(n)-1/2}, x_{m(n)+1/2}). \quad (3.30)$$

At a time t^n the moving mesh is defined by the points

$$x_{j-1/2}^n := \begin{cases} x_{j-1/2}, & j \leq m(n) - 1 \text{ or } j \geq m(n) + 2, \\ \xi^n, & j = m(n), m(n) + 1. \end{cases} \quad (3.31)$$

The computational cells in the moving mesh at each time t^n are defined by

$$j \neq m(n), \quad |j| \leq \frac{1}{h}, \quad \mathbf{C}_j^n := [x_{j-1/2}^n, x_{j+1/2}^n] = \begin{cases} C_j, & |j - m(n)| \geq 2 \\ D_L^n, & j = m(n) - 1, \\ D_R^n, & j = m(n) + 1, \end{cases} \quad (3.32)$$

where

$$D_L^n := \mathbf{C}_{m(n)-1}^n = [x_{m(n)-3/2}^n, \xi^n], \quad D_R^n := \mathbf{C}_{m(n)+1}^n = [\xi^n, x_{m(n)+3/2}^n]. \quad (3.33)$$

The length of the computational cells \mathbf{C}_j^n in the moving mesh is given by

$$j \neq m(n), \quad h_j^n := |\mathbf{C}_j^n| = \begin{cases} h, & |j - m(n)| \geq 2 \\ \Delta_L^n, & j = m(n) - 1, \\ \Delta_R^n, & j = m(n) + 1, \end{cases} \quad (3.34)$$

where, after (3.30) and (3.33), the quantities $\Delta_L^n := |D_L^n|$, $\Delta_R^n := |D_R^n|$ satisfy

$$\Delta_L^n + \Delta_R^n = 3h, \quad h \leq \Delta_L^n, \quad \Delta_R^n \leq 2h. \quad (3.35)$$

We stress that ξ^n is a point of the grid at time t^n and that it corresponds to the lumped indexes $m(n) \pm 1$. Therefore, the two nearby cells around the value ξ^n correspond to three cells in the reference mesh. Comparing with (3.27), we notice that

$$\bigcup_{j=-1/h, j \neq m(n)}^{1/h} \mathbf{C}_j^n = \left[-\frac{h}{2} - 1, 1 + \frac{h}{2} \right). \quad (3.36)$$

3.2 Time evolution of the grid

Here we consider the time variation of the grid from t^n to t^{n+1} . By assuming the CFL condition

$$k \max \{ \|f'\|_\infty, \|\xi'\|_\infty \} \leq \frac{h}{2}, \quad (3.37)$$

and recalling (3.29), we find that

$$|\xi^{n+1} - \xi^n| \leq k \|\xi'\|_\infty \leq \frac{h}{2}$$

and therefore the map $\xi^k(t)$ crosses at most one boundary cell of the reference mesh. That is, at $t = t^{n+1}$ one has

$$m(n+1) \in \{m(n), m(n) \pm 1\}.$$

Here we analyze the variation of the mesh, given in Definition 3.1, from time t^n to t^{n+1} in the various cases.

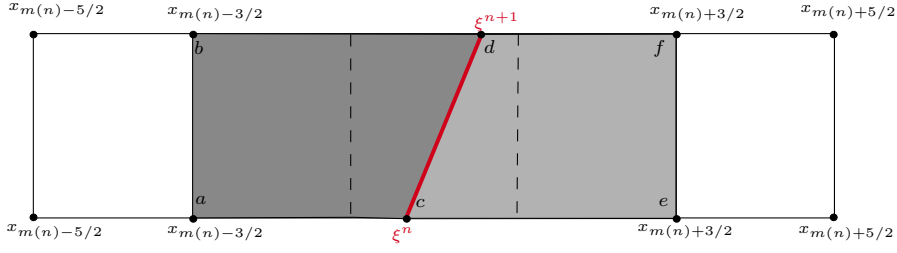


Fig. 2 Illustration of mesh adaptation for Case A

Case A: $m(n) = m(n+1)$ In this case $x_{j-1/2}^{n+1} = x_{j-1/2}^n$ for $j \neq m(n), m(n)+1$ and the point ξ^n moves to ξ^{n+1} . In particular:

$$\begin{aligned} t^{n+1} : & \quad x_{m(n+1)-3/2}, & \quad \xi^{n+1}, & \quad x_{m(n+1)+3/2}; \\ t^n : & \quad x_{m(n)-3/2}, & \quad \xi^n, & \quad x_{m(n)+5/2}. \end{aligned}$$

The values of Δ_L^n , Δ_L^{n+1} and of Δ_R^n , Δ_R^{n+1} satisfy the relations

$$\Delta_L^{n+1} = \Delta_L^n + \alpha_{n,k}k, \quad \Delta_R^{n+1} = \Delta_R^n - \alpha_{n,k}k. \quad (3.38)$$

See Figure 2.

Case B: $m(n+1) = m(n) + 1$ Here the line joining (ξ^n, t^n) and (ξ^{n+1}, t^{n+1}) crosses the vertical line $x = x_{m(n)+1/2}$ of the reference mesh. See Figure 3.

To illustrate the mesh change from time t^n to t^{n+1} , let us consider the points corresponding to the four indexes $j = m(n) - 1, \dots, m(n) + 2$:

$$\begin{aligned} t^{n+1} : & \quad x_{m(n+1)-5/2}, & \quad x_{m(n+1)-3/2}, & \quad \xi^{n+1}, & \quad x_{m(n+1)+3/2}; \\ t^n : & \quad x_{m(n)-3/2}, & \quad \xi^n, & \quad x_{m(n)+3/2}, & \quad x_{m(n)+5/2}. \end{aligned}$$

Note that the grid point $x_{m(n)-1/2} = x_{m(n+1)-3/2}$ is present at time t^{n+1} and not at time t^n , whereas the grid point $x_{m(n)+3/2} = x_{m(n+1)+1/2}$ is present at time t^n but it is excluded from the mesh at t^{n+1} .

The following identities hold:

$$h + \Delta_L^{n+1} = \Delta_L^n + \alpha_{n,k}k, \quad \Delta_R^{n+1} = \Delta_R^n - \alpha_{n,k}k + h. \quad (3.39)$$

Case C: $m(n+1) = m(n) - 1$ This case is possible only if $\alpha_{n,k} < 0$ and is peculiar to case B:

$$\begin{aligned} t^{n+1} : & \quad x_{m(n+1)-3/2}, & \quad \xi^{n+1}, & \quad x_{m(n+1)+3/2}, & \quad x_{m(n+1)+5/2}; \\ t^n : & \quad x_{m(n)-5/2}, & \quad x_{m(n)-3/2}, & \quad \xi^n, & \quad x_{m(n)+3/2}. \end{aligned}$$

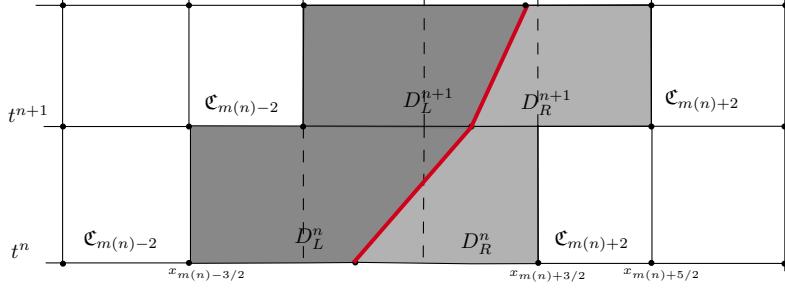


Fig. 3 Case B. Dashed lines indicate that the corresponding cell boundary is removed.

The following identities hold:

$$\Delta_L^{n+1} = \Delta_L^n + \alpha_{n,k} \mathbf{k} + \mathbf{h}, \quad \mathbf{h} + \Delta_R^{n+1} = \Delta_R^n - \alpha_{n,k} \mathbf{k}. \quad (3.40)$$

3.3 The numerical fluxes

In this subsection, we introduce the numerical fluxes employed in the scheme.

Define

$$h^\pm(a, b) := \begin{cases} \min_{[a,b]}(\pm f), & \text{if } a \leq b, \\ \max_{[b,a]}(\pm f), & \text{if } a \geq b \end{cases} \quad (3.41)$$

and, for $\alpha \in \mathbb{R}$,

$$h_0(a, b, \alpha) = \begin{cases} f(b) - \alpha b = -b(\alpha - v(b)), & \text{if } \alpha \geq v(b), \\ -f(a) - \alpha a = a(-\alpha - v(a)), & \text{if } \alpha \leq -v(a) \\ 0, & \text{otherwise,} \end{cases} \quad (3.42)$$

or equivalently

$$h_0(a, b, \alpha) = -b[v(b) - \alpha]_- + a[v(a) + \alpha]_-, \quad (3.43)$$

where $[x]_- = \max\{-x, 0\}$.

The maps h^\pm represent the Godunov fluxes at a vertical boundary of a cell, corresponding to the fluxes $\pm f$ respectively, while the map $h_0 : [0, 1] \times [0, 1] \times \mathbb{R}$ represents the flux along the possibly non-vertical boundary cell with slope α .

Notice that

$$h^-(a, b) = - \begin{cases} \max_{[a,b]} f, & \text{if } a \leq b, \\ \min_{[b,a]} f, & \text{if } a \geq b, \end{cases}$$

and hence $h^-(a, b) = -h^+(b, a)$.

Moreover, the maps h^\pm , h_0 are Lipschitz continuous with Lipschitz constant

$$Lip(h^\pm) \leq \|f'\|_\infty, \quad Lip(h_0) \leq \|f'\|_\infty + |\alpha|. \quad (3.44)$$

We stress that the numerical fluxes h^\pm , h_0 are based on the exact Riemann solver at the interface. See Section 2.1. In the following lemma, we provide some monotonicity properties of the numerical fluxes and the value of h_0 when its arguments (a, b, α) satisfy the Rankine-Hugoniot condition (2.20) at the flux interface.

Lemma 3.2. *For any given a and b in $[0, 1]$ the following hold*

- (i) $h^\pm(a, a) = \pm f(a)$,
- (ii) $h^\pm(a, b)$ and $h_0(a, b, \alpha)$ are nondecreasing with respect to a and nonincreasing with respect to b , for all $\alpha \in \mathbb{R}$,
- (iii) $h_0(a, b, 0) = 0$,
- (iv) for all α ,

$$h_0(a, a, \alpha) = \begin{cases} -\alpha a + f(a), & \text{if } \alpha \geq v(a), \\ -\alpha a - f(a), & \text{if } \alpha \leq -v(a), \\ 0, & \text{otherwise.} \end{cases} \quad (3.45)$$

- (v) If

$$f(b) + f(a) = \alpha(b - a), \quad (3.46)$$

then

$$h_0(a, b, \alpha) = f(b) - \alpha b = -\alpha a - f(a). \quad (3.47)$$

Proof. All of the properties (i)–(iv) are direct consequences of the definitions in (3.41)–(3.43) and the fact that the map $\rho \mapsto \rho[v(\rho) + \text{const.}]_-$ is nondecreasing, being the composition of two nonincreasing maps.

Concerning (v), by (3.43) and (3.46)

$$\begin{aligned} h_0(a, b, \alpha) &= -[\alpha b - f(b)]_+ + [\alpha a + f(a)]_- \\ &= -[\alpha b - f(b)]_+ + [\alpha b - f(b)]_- \\ &= -\alpha b + f(b), \end{aligned}$$

where we used the identity $[x]_+ - [x]_- = x$. Hence we get the first equality in (3.47); the second one follows immediately from (3.46). \square

3.4 The numerical scheme

In this subsection we define a family of approximate solution to (1.1). We assume the notation of Definition 3.1 and the CFL condition (3.37) for the space and time steps h and k .

The approximate solution $\rho^h(x, t)$, at time t^n , takes the form

$$\rho^h(x, t^n) = \rho_j^n \quad x \in C_j^n, \quad j \neq m(n), \quad |j| \leq \frac{1}{h}, \quad n \geq 0 \quad (3.48)$$

for suitable values ρ_j^n to be defined and $j \in \mathbb{Z}$. In addition, we take into account the boundary conditions by considering two extra values for the density:

$$\rho_{\pm(1+1/h)}^n = 0, \quad n \geq 0 \quad (3.49)$$

on the two extra cells

$$C_{-\frac{1}{h}-1} := \left[x_{-\frac{1}{h}-\frac{3}{2}}, x_{-\frac{1}{h}-\frac{1}{2}} \right), \quad C_{1+\frac{1}{h}} := \left[x_{\frac{1}{h}+\frac{1}{2}}, x_{\frac{1}{h}+\frac{3}{2}} \right).$$

For convenience, we will use the notation

$$\rho_L^n := \rho_{m(n)-1}^n, \quad \rho_R^n := \rho_{m(n)+1}^n. \quad (3.50)$$

Let's proceed with the definition of the values ρ_j^n .

Initialization: At $t = 0$ the initial data $\rho_0(x) \in L^\infty(-1, 1)$ is discretized by the local average on the cell:

$$\rho_j^0 = \frac{1}{h_j^0} \int_{C_j^0} \rho_0(x) dx, \quad j \neq m(0), \quad (3.51)$$

with C_j^0, h_j^0 as in (3.32), (3.34) for $n = 0$.

Iteration step: Assume that the ρ_j^n are known for some $n \geq 0$ and $|j| \leq 2^N, j \neq m(n)$, and that (3.49) holds.

Having set $\rho^h(x, t^n)$ as in (3.48) and recalling $\xi^k(t)$ from (3.29), the solution ρ^h is prolonged for $t \in (t^n, t^{n+1})$ as the *exact* solution of the problem

$$\begin{cases} \partial_t \rho + \partial_x \{ \text{sign}(x - \xi^k(t)) f(\rho) \} = 0, \\ \rho(x, t^n) = \rho^h(x, t^n) \end{cases} \quad (3.52)$$

on the set $(-\frac{3}{2}h - 1, 1 + \frac{3}{2}h)$.

Notice that, thanks to (3.49), the following condition is satisfied:

$$\rho^h(t, \pm(1 + h/2)) \in [0, \text{argmax}_{[0,1]} f] \quad (3.53)$$

and this will serve as the boundary condition for the original problem. See [4, 32].

Now, we define the values

$$\rho_j^{n+1}, \quad j \in \left\{ -\frac{1}{h}, \dots, \frac{1}{h} \right\} \setminus \{m(n+1)\}$$

in the Cases **A**, **B** and **C**, as follows.

Case A: $m(n) = m(n+1)$ Here, with the notation of (3.34), we set

$$\rho_j^{n+1} := \frac{1}{h_j^{n+1}} \int_{C_j^{n+1}} \rho^h(x, t^{n+1}-) dx, \quad j \neq m(n+1). \quad (3.54)$$

In particular, we have the following values

- For $|j - m(n)| \geq 2$ the boundary of the cells are vertical and the ρ_j^{n+1} are defined in a standard way: for $-1/h \leq j \leq m(n+1) - 2$,

$$\rho_j^{n+1} = \rho_j^n - \frac{k}{h} \cdot [h^-(\rho_j^n, \rho_{j+1}^n) - h^-(\rho_{j-1}^n, \rho_j^n)] \quad (3.55)$$

while for $m(n+1) + 2 \leq j \leq 1/h$:

$$\rho_j^{n+1} = \rho_j^n - \frac{k}{h} \cdot [h^+(\rho_j^n, \rho_{j+1}^n) - h^+(\rho_{j-1}^n, \rho_j^n)] . \quad (3.56)$$

Notice that for the extreme values of the indexes $j = \pm 1/h$ we use the extended values (3.49); for instance, if $j = 1/h$ then (3.56) reduces to

$$\rho_{1/h}^{n+1} = \rho_{1/h}^n - \frac{k}{h} \cdot [h^+(\rho_{1/h}^n, 0) - h^+(\rho_{1/h-1}^n, \rho_{1/h}^n)] .$$

- For $j = m(n) - 1$ we consider the trapezoid in the (x, t) -plane with corners

$$(x_{m(n)-3/2}, t^n), \quad (\xi^n, t^n), \quad (\xi^{n+1}, t^{n+1}), \quad (x_{m(n)-3/2}, t^{n+1});$$

It can be observed that, using the notation given in equation (3.33), the lower basis is D_L^n and the upper basis is $C_{m(n)-1}^n = D_L^{n+1}$. Then we integrate $\rho^h(x, t)$ over the trapezoid to get

$$\begin{aligned} & \int_{D_L^{n+1}} \rho^h(x, t^{n+1}-) dx - \int_{D_L^n} \rho^h(x, t^n+) dx \\ & + \int_{t^n}^{t^{n+1}} h_0(\rho_L^n, \rho_R^n, \alpha_{n,k}) dt - \int_{t^n}^{t^{n+1}} h^-(\rho_{m(n)-2}^n, \rho_L^n) dt = 0, \end{aligned}$$

that is

$$\Delta_L^{n+1} \rho_L^{n+1} = \Delta_L^n \rho_L^n - k [h_0(\rho_L^n, \rho_R^n, \alpha_{n,k}) - h^-(\rho_{m(n)-2}^n, \rho_L^n)], \quad (3.57)$$

where Δ_L^n is defined at (3.34). By recalling (3.38), the formula here above can be rewritten as

$$\rho_L^{n+1} = \rho_L^n - \frac{k}{\Delta_L^{n+1}} [h_0(\rho_L^n, \rho_R^n, \alpha_{n,k}) - h^-(\rho_{m(n)-2}^n, \rho_L^n) + \alpha_{n,k} \rho_L^n] .$$

- For $j = m(n) + 1$, we proceed similarly as the previous case and define

$$\Delta_R^{n+1} \rho_R^{n+1} = \Delta_R^n \rho_R^n - k [h^+(\rho_R^n, \rho_{m(n)+2}^n) - h_0(\rho_L^n, \rho_R^n, \alpha_{n,k})], \quad (3.58)$$

with $\Delta_R^{n+1} = \Delta_R^n - \alpha_{n,k} k$, see (3.38)₂. Consequently, we obtain

$$\rho_R^{n+1} = \rho_R^n - \frac{k}{\Delta_R^{n+1}} [h^+(\rho_R^n, \rho_{m(n)+2}^n) - h_0(\rho_L^n, \rho_R^n, \alpha_{n,k}) - \alpha_{n,k} \rho_R^n] .$$

Case B: $m(n+1) = m(n) + 1$ We focus on the region in the time interval $[t^n, t^{n+1}]$ which is delimited by the cell points

$$x_{m(n)-3/2} = x_{m(n+1)-5/2}, \quad x_{m(n)+5/2} = x_{m(n+1)+3/2}.$$

At time t^n the region above corresponds to three cells and three corresponding values of the density

$$D_L^n, \rho_L^n; \quad D_R^n, \rho_R^n; \quad C_{m(n)+2}^n, \rho_{m(n)+2}^n.$$

On the other hand, at time t^{n+1} the cells and values in the region are:

$$C_{m(n+1)-2}^{n+1}, \rho_{m(n+1)-2}^{n+1}; \quad D_L^{n+1}, \rho_L^{n+1}; \quad D_R^{n+1}, \rho_R^{n+1}. \quad (3.59)$$

Now we set

$$\rho_{m(n+1)-2}^{n+1} = \rho_L^{n+1} := \bar{\rho}, \quad (3.60)$$

where the value $\bar{\rho}$ is defined by the integration on the trapezoid delimited by $x_{m(n)-3/2} = x_{m(n+1)-5/2}$ and the segment connecting (ξ^n, t^n) to (ξ^{n+1}, t^{n+1}) , as follows:

$$(h + \Delta_L^{n+1}) \bar{\rho} = \Delta_L^n \rho_L^n - k \left[h_0(\rho_L^n, \rho_R^n, \alpha_{n,k}) - h^- \left(\rho_{m(n)-2}^n, \rho_L^n \right) \right]. \quad (3.61)$$

By using the identity (3.39)₁, we find that

$$\rho_L^{n+1} = \rho_L^n - \frac{k}{h + \Delta_L^{n+1}} \left[h_0(\rho_L^n, \rho_R^n, \alpha_{n,k}) - h^- \left(\rho_{m(n)-2}^n, \rho_L^n \right) + \alpha_{n,k} \rho_L^n \right].$$

For the definition of ρ_R^{n+1} , we proceed similarly by integration on the trapezoid on the right of the segment connecting (ξ^n, t^n) to (ξ^{n+1}, t^{n+1}) : we obtain that it is defined by the identity

$$\Delta_R^{n+1} \rho_R^{n+1} = \Delta_R^n \rho_R^n + h \rho_{m(n)+2}^n - k \left[h^+ \left(\rho_{m(n)+2}^n, \rho_{m(n)+3}^n \right) - h_0(\rho_L^n, \rho_R^n, \alpha_{n,k}) \right]. \quad (3.62)$$

By means of the identity (3.39)₂ we rewrite (3.62) as follows:

$$\begin{aligned} \rho_R^{n+1} &= \frac{\Delta_R^{n+1} - h}{\Delta_R^{n+1}} \rho_R^n + \frac{h}{\Delta_R^{n+1}} \rho_{m(n)+2}^n \\ &\quad - \frac{k}{\Delta_R^{n+1}} \left[h^+ \left(\rho_{m(n)+2}^n, \rho_{m(n)+3}^n \right) - h_0(\rho_L^n, \rho_R^n, \alpha_{n,k}) - \alpha_{n,k} \rho_R^n \right]. \end{aligned}$$

This completes the definition of the three values in (3.59), that is, for ρ_j^{n+1} with $j = m(n+1) - 2$ and $j = m(n+1) \pm 1$.

On the other hand, the values ρ_j^{n+1} for $j \leq m(n+1) - 3$ and $j \geq m(n+1) + 2$ are given by the standard formulas (3.55), (3.56) respectively.

This completes the definition of the values ρ_j^{n+1} with $j \neq m(n+1)$ for Case B.

Case C: $m(n+1) = m(n) - 1$ In this case, we focus on the region in the time interval $[t^n, t^{n+1}]$, which is delimited by the cell points

$$x_{m(n)-5/2} = x_{m(n+1)-3/2}, \quad x_{m(n)+3/2} = x_{m(n+1)+5/2}.$$

At time t^n , the region above corresponds to three cells and three corresponding values:

$$C_{m(n)-2}^n, \rho_{m(n)-2}^n; \quad D_L^n, \rho_L^n; \quad D_R^n, \rho_R^n.$$

On the other hand, at time t^{n+1} the cells and values in the region are:

$$D_L^{n+1}, \rho_L^{n+1}; \quad D_R^{n+1}, \rho_R^{n+1}; \quad C_{m(n+1)+2}^{n+1}, \rho_{m(n+1)+2}^{n+1}. \quad (3.63)$$

The marching formulas which allow us to compute the values of $\rho_L^{n+1}, \rho_R^{n+1}, \rho_{m(n+1)+2}^{n+1}$, are mirror images of the ones in (3.60)–(3.62), as the only difference between the two cases is the sign of $\alpha_{n,k}$ (positive in Case **B**, negative in Case **C**). For the reader's convenience, we write them explicitly.

$$\Delta_L^{n+1} \rho_L^{n+1} = \Delta_L^n \rho_L^n + h \rho_{m(n)-2}^n - k \left[h_0(\rho_L^n, \rho_R^n, \alpha_{n,k}) - h^- \left(\rho_{m(n)-3}^n, \rho_{m(n)-2}^n \right) \right]. \quad (3.64)$$

Now, we set

$$\rho_R^{n+1} = \rho_{m(n+1)+2}^{n+1} := \bar{\rho}, \quad (3.65)$$

where the value $\bar{\rho}$ is defined by

$$(h + \Delta_R^{n+1}) \bar{\rho} = \Delta_R^n \rho_R^n - k \left[h^+ \left(\rho_R^n, \rho_{m(n)+2}^n \right) - h_0(\rho_L^n, \rho_R^n, \alpha_{n,k}) \right].$$

The values ρ_j^{n+1} for $j \leq m(n+1) - 2$ and $j \geq m(n+1) + 3$ are given by the standard formulas (3.55), (3.56) respectively.

This completes the definition of the values ρ_j^{n+1} with $j \neq m(n+1)$ for Case **C**.

4 Analysis of the scheme

In this section, we analyze the scheme and prove relevant properties that provide a strong basis to establish its convergence to the entropy solution defined in Section 2. For convenience, we rewrite the equation (1.1) here as:

$$\begin{cases} \partial_t \rho + \partial_x \{ \text{sign}(x - \xi(t)) f(\rho) \} = 0, \\ \rho(\cdot, 0) = \rho_0, \\ \rho(t, \pm 1) \in [0, \text{argmax}_{[0,1]} f] \end{cases} \quad (4.66)$$

with $\xi(t)$ satisfying (1.4).

Let's start by introducing a convenient expression of the scheme that will be useful during the analysis. We define

$$H^\pm(a, b, c; \mathbf{k}, \mathbf{h}) = b - \frac{\mathbf{k}}{\mathbf{h}} [h^\pm(b, c) - h^\pm(a, b)], \quad (4.67)$$

$$H_L^{AB}(a, b, c; \mathbf{k}, \Delta_L, \alpha) = \frac{\Delta_L}{\Delta_L + \alpha \mathbf{k}} b - \frac{\mathbf{k}}{\Delta_L + \alpha \mathbf{k}} (h_0(b, c, \alpha) - h^-(a, b)) \quad (4.68)$$

$$H_R^{AC}(a, b, c; \mathbf{k}, \Delta_R, \alpha) = \frac{\Delta_R}{\Delta_R - \alpha \mathbf{k}} b - \frac{\mathbf{k}}{\Delta_R - \alpha \mathbf{k}} (h^+(b, c) - h_0(a, b, \alpha)), \quad (4.69)$$

and

$$H_L^C(a, b, c, d; \mathbf{k}, \mathbf{h}, \Delta_L, \alpha) = \frac{\Delta_L}{\Delta_L + \mathbf{h} + \alpha \mathbf{k}} b + \frac{\mathbf{h}}{\Delta_L + \mathbf{h} + \alpha \mathbf{k}} c - \frac{\mathbf{k}}{\Delta_L + \mathbf{h} + \alpha \mathbf{k}} (h_0(c, d, \alpha) - h^-(a, b)), \quad (4.70)$$

$$H_R^B(a, b, c, d; \mathbf{k}, \mathbf{h}, \Delta_R, \alpha) = \frac{\Delta_R}{\Delta_R + \mathbf{h} - \alpha \mathbf{k}} b + \frac{\mathbf{h}}{\Delta_R + \mathbf{h} - \alpha \mathbf{k}} c - \frac{\mathbf{k}}{\Delta_R + \mathbf{h} - \alpha \mathbf{k}} (h^+(c, d) - h_0(a, b, \alpha)). \quad (4.71)$$

Then the expressions (3.55)–(3.58), Case **A**, can be rewritten as

$$\rho_j^{n+1} = \begin{cases} H^-(\rho_{j-1}^n, \rho_j^n, \rho_{j+1}^n; \mathbf{k}, \mathbf{h}), & -1/\mathbf{h} \leq j \leq m(n+1) - 2, \\ H^+(\rho_{j-1}^n, \rho_j^n, \rho_{j+1}^n; \mathbf{k}, \mathbf{h}), & m(n+1) + 2 \leq j \leq 1/\mathbf{h}, \end{cases} \quad (4.72)$$

and

$$\rho_j^{n+1} = \begin{cases} H_L^{AB}(\rho_{m(n)-2}^n, \rho_L^n, \rho_R^n; \mathbf{k}, \Delta_L^n, \alpha_{n,\mathbf{k}}), & j = m(n+1) - 1, \\ H_R^{AC}(\rho_L^n, \rho_R^n, \rho_{m(n)+2}^n; \mathbf{k}, \Delta_R^n, \alpha_{n,\mathbf{k}}), & j = m(n+1) + 1. \end{cases} \quad (4.73)$$

The corresponding expressions for the Case **B** write as

$$\rho_j^{n+1} = \begin{cases} H^-(\rho_{j-1}^n, \rho_j^n, \rho_{j+1}^n; \mathbf{k}, \mathbf{h}), & -\frac{1}{\mathbf{h}} \leq j \leq m(n+1) - 3, \\ H^+(\rho_{j-1}^n, \rho_j^n, \rho_{j+1}^n; \mathbf{k}, \mathbf{h}), & m(n+1) + 2 \leq j \leq \frac{1}{\mathbf{h}}, \end{cases} \quad (4.74)$$

and

$$\rho_j^{n+1} = \begin{cases} H_L^{AB}(\rho_{m(n)-2}^n, \rho_L^n, \rho_R^n; \mathbf{k}, \Delta_L^n, \alpha_{n,\mathbf{k}}), & j = m(n+1) - 2, \\ & m(n+1) - 1, \\ H_R^B(\rho_L^n, \rho_R^n, \rho_{m(n)+2}^n, \rho_{m(n)+3}^n; \mathbf{k}, \mathbf{h}, \Delta_R^n, \alpha_{n,\mathbf{k}}), & j = m(n+1) + 1. \end{cases} \quad (4.75)$$

Finally, for the Case **C** we have

$$\rho_j^{n+1} = \begin{cases} H^-(\rho_{j-1}^n, \rho_j^n, \rho_{j+1}^n; \mathbf{k}, \mathbf{h}), & -2^N \leq j \leq m(n+1) - 2, \\ H^+(\rho_{j-1}^n, \rho_j^n, \rho_{j+1}^n; \mathbf{k}, \mathbf{h}), & m(n+1) + 3 \leq j \leq 2^N, \end{cases} \quad (4.76)$$

and

$$\rho_j^{n+1} = \begin{cases} H_L^C(\rho_{m(n)-3}^n, \rho_{m(n)-2}^n, \rho_L^n, \rho_R^n; \mathbf{k}, \mathbf{h}, \Delta_L^n, \alpha_{n,\mathbf{k}}), & j = m(n+1) - 1, \\ H_R^{AC}(\rho_L^n, \rho_R^n, \rho_{m(n)+2}^n; \mathbf{k}, \Delta_R^n, \alpha_{n,\mathbf{k}}), & j = m(n+1) + 1, \\ & m(n+1) + 2. \end{cases} \quad (4.77)$$

In the following lemma, we establish some monotonicity properties of the maps defined at (4.67)–(4.71).

Lemma 4.1. *Given that the CFL condition (3.37) is satisfied, the functions H^\pm , H_L^{AB} and H_R^{AC} are nondecreasing with respect to their first three arguments a, b, c .*

The functions H_L^C and H_R^B are nondecreasing with respect of their first four arguments a, b, c, d .

Proof. The functions H^\pm , H_L^{AB} , H_R^{AC} , H_R^B , and H_L^C are Lipschitz continuous; therefore, we can check their monotonicity properties by computing a.e. the partial derivatives. To keep our presentation as light as possible, we provide detailed estimates only for H_R^B , see (4.71), as the other cases are very similar.

Thanks to Lemma 3.2, the CFL condition (3.37) and the fact that $\mathbf{h} \leq \Delta_R \leq 2\mathbf{h}$, we have that

$$\begin{aligned} \partial_a H_R^B(a, b, c, d; \mathbf{k}, \mathbf{h}, \Delta_R, \alpha) &= \frac{\mathbf{k}}{\Delta_R + \mathbf{h} - \alpha \mathbf{k}} \partial_a h_0(a, b, \alpha) \geq 0, \\ \partial_b H_R^B(a, b, c, d; \mathbf{k}, \mathbf{h}, \Delta_R, \alpha) &= \frac{\Delta_R}{\Delta_R + \mathbf{h} - \alpha \mathbf{k}} - \frac{\mathbf{k}}{\Delta_R + \mathbf{h} - \alpha \mathbf{k}} |\partial_b h_0(a, b, \alpha)| \\ &\geq \frac{1}{2} \frac{2\Delta_R - \mathbf{h}}{\Delta_R + \mathbf{h} - \alpha \mathbf{k}} > 0, \\ \partial_c H_R^B(a, b, c, d; \mathbf{k}, \mathbf{h}, \Delta_R, \alpha) &= \frac{\mathbf{h}}{\Delta_R + \mathbf{h} - \alpha \mathbf{k}} - \frac{\mathbf{k}}{\Delta_R + \mathbf{h} - \alpha \mathbf{k}} \partial_c h^+(c, d) \\ &\geq \frac{1}{2} \frac{\mathbf{h}}{\Delta_R + \mathbf{h} - \alpha \mathbf{k}} > 0, \\ \partial_d H_R^B(a, b, c, d; \mathbf{k}, \mathbf{h}, \Delta_R, \alpha) &= \frac{\mathbf{k}}{\Delta_R + \mathbf{h} - \alpha \mathbf{k}} |\partial_d h^+(c, d)| \geq 0. \end{aligned}$$

□

For future use, we define the remainder terms

$$\mathbf{R}_L(b, \alpha) = \begin{cases} 0, & \text{if } \alpha \leq -v(b), \\ f(b) + \alpha b, & \text{if } \alpha \in (-v(b), v(b)), \\ 2f(b), & \text{if } \alpha \geq v(b), \end{cases} \quad (4.78)$$

and $\mathbf{R}_R(b, \alpha) := 2f(b) - \mathbf{R}_L(b, \alpha)$. Observe that the remainder terms are always non negative.

Let us now collect other useful properties of the maps defined at (4.67)–(4.71).

Lemma 4.2. For any $b \in [0, 1]$ we have

$$H^\pm(b, b, b; k, h) = b, \quad (4.79)$$

$$H_L^{AB}(b, b, b; k, h, \alpha) = b - \frac{k}{\Delta_L + \alpha k} R_L(b, \alpha) \leq b, \quad (4.80)$$

$$H_L^C(b, b, b, b; k, h, \Delta_L, \alpha) = b - \frac{k}{\Delta_L + h + \alpha k} R_L(b, \alpha),$$

$$H_R^{AC}(b, b, b; k, h, \alpha) = b - \frac{k}{\Delta_R - \alpha k} R_R(b, \alpha), \quad (4.81)$$

$$H_R^B(b, b, b, b; k, h, \Delta_R, \alpha) = b - \frac{k}{\Delta_R + h - \alpha k} R_R(b, \alpha). \quad (4.82)$$

Moreover, if b and c satisfy the Rankine-Hugoniot condition, namely $f(b) + f(c) = \alpha(c - b)$, then

$$H_L^{AB}(b, b, c; k, \Delta_L, \alpha) = H_L^C(b, b, b, c; k, h, \Delta_L, \alpha) = b,$$

$$H_R^{AC}(b, c, c; k, \Delta_R, \alpha) = H_R^B(b, c, c, c; k, h, \Delta_R, \alpha) = c.$$

Proof. These properties are direct consequences of Lemma 3.2 and of the identities

$$h_0(b, b, \alpha) - h^-(b, b) = -\alpha b + R_L(b, \alpha), \quad h^+(b, b) - h_0(b, b, \alpha) = -\alpha b + R_R(b, \alpha).$$

□

Proposition 4.1. (Uniform L^∞ bounds). Let $\rho_{\max} = \|\rho_0\|_\infty$. For any $(t, x) \in [0, T] \times [-1, 1]$, the numerical solution ρ^h satisfies the bounds

$$0 \leq \rho^h(x, t) \leq \|\rho_0\|_\infty. \quad (4.83)$$

Proof. At $t = 0$, the property (4.83) holds by the definition (3.51) of the ρ_j^0 . If the property holds up to $t = nk$ then all the densities ρ_j^{n+1} , for $-2^N \leq j \leq 2^N$, $j \neq m(n+1)$, are the values of one of the functions H^\pm , H_L^{AB} , H_R^{AC} , H_R^B and H_L^C . Then, in Case **B** we have

$$\underbrace{H^+(0, 0, 0; k, h)}_{=0} \leq \underbrace{H^+(\rho_{j-1}^n, \rho_j^n, \rho_{j+1}^n; k, h)}_{=\rho_j^{n+1}} \leq \underbrace{H^+(\rho_{\max}, \rho_{\max}, \rho_{\max}; k, h)}_{=\rho_{\max}}$$

$$\begin{aligned} \underbrace{H_L^{AB}(0, 0, 0; k, h, \alpha_{n,k})}_{=0} &\leq \underbrace{H_L^{AB}(\rho_{m(n)-2}^n, \rho_L^n, \rho_R^n; k, h, \alpha_{n,k})}_{=\rho_L^{n+1}} \\ &\leq \underbrace{H_L^{AB}(\rho_{\max}, \rho_{\max}, \rho_{\max}; k, h, \alpha_{n,k})}_{=\rho_{\max} - \frac{k}{\Delta_L + \alpha k} R_L(b, \alpha)} \leq \rho_{\max}, \end{aligned}$$

$$\begin{aligned}
\underbrace{H_R^B(0, 0, 0, 0; \mathbf{k}, \mathbf{h}, \Delta_R, \alpha_{n,k})}_{=0} &\leq \underbrace{H_R^B(\rho_L^n, \rho_R^n, \rho_{m(n)+2}^n, \rho_{m(n)+3}^n; \mathbf{k}, \mathbf{h}, \Delta_R, \alpha_{n,k})}_{=\rho_R^{n+1}} \\
&\leq \underbrace{H_R^B(\rho_{\max}, \rho_{\max}, \rho_{\max}, \rho_{\max}; \mathbf{k}, \mathbf{h}, \Delta_R, \alpha_{n,k})}_{=\rho_{\max} - \frac{k}{\Delta_R^{n+1}} R_R(b, \alpha)} \leq \rho_{\max}.
\end{aligned}$$

Cases **A** and **C** are similar. Therefore, the inequalities in (4.83) hold by induction. \square

4.1 Approximate entropy inequalities

In the following lemma, we introduce a discrete version of entropy inequalities. As in a large part of the literature, we consider the family of Kruzhkov entropies $\eta_k(\rho) = |\rho - k|$, for $k \in [0, 1]$ and introduce suitable discrete entropy fluxes. In particular, we write

$$\begin{aligned}
Q_j^{\pm, n} &= h^\pm(\rho_{j-1}^n \vee k, \rho_j^n \vee k) - h^\pm(\rho_{j-1}^n \wedge k, \rho_j^n \wedge k), \\
Q_0^n &= h_0(\rho_L^n \vee k, \rho_R^n \vee k, \alpha_{n,k}) - h_0(\rho_L^n \wedge k, \rho_R^n \wedge k, \alpha_{n,k}).
\end{aligned}$$

In the next lemma, we deduce entropy inequalities valid for each cell.

Lemma 4.3. (Discrete entropy inequalities).

Fix $k \in [0, 1]$, $n \in \mathbb{N}$ and $j \in \{-\frac{1}{h}, \dots, \frac{1}{h}\}$ with $j \neq m(n+1)$. Then the following holds.

Case A: If $j \leq m(n+1) - 2$ and $j \geq m(n+1) + 2$, then

$$h|\rho_j^{n+1} - k| \leq h|\rho_j^n - k| - k(Q_{j+1}^{\pm, n} - Q_j^{\pm, n}) \quad (4.84)$$

and

$$\Delta_L^{n+1}|\rho_L^{n+1} - k| \leq \Delta_L^n|\rho_L^n - k| - k(Q_0^n - Q_{m(n)-1}^{-, n}) + kR_L(k, \alpha_{n,k}), \quad (4.85)$$

$$\Delta_R^{n+1}|\rho_R^{n+1} - k| \leq \Delta_R^n|\rho_R^n - k| - k(Q_{m(n)+2}^{+, n} - Q_0^n) + kR_R(k, \alpha_{n,k}). \quad (4.86)$$

Case B: The inequality (4.84) holds for $j \leq m(n+1) - 3$ and $j \geq m(n+1) + 2$. Moreover, the following analogous of inequalities (4.85), (4.86) are satisfied:

$$(\Delta_L^{n+1} + h)|\bar{\rho} - k| \leq \Delta_L^n|\rho_L^n - k| - k(Q_0^n - Q_{m(n)-1}^{-, n}) + kR_L(k, \alpha_{n,k}), \quad (4.87)$$

and

$$\begin{aligned}
\Delta_R^{n+1}|\rho_R^{n+1} - k| &\leq \Delta_R^n|\rho_R^n - k| + h|\rho_{m(n)+2}^n - k| \\
&\quad - k(Q_{m(n)+3}^{+, n} - Q_0^n) + kR_R(k, \alpha_{n,k})
\end{aligned} \quad (4.88)$$

where $\bar{\rho}$ is defined at (3.61).

Case C: The inequality (4.84) holds for $j \leq m(n+1) - 2$ and $j \geq m(n+1) + 3$. Moreover, the following analogous of inequalities (4.85), (4.86) are satisfied:

$$(\Delta_R^{n+1} + h)|\bar{\rho} - k| \leq \Delta_R^n|\rho_R^n - k| - k(Q_{m(n)+2}^{+, n} - Q_0^n) + kR_R(k, \alpha_{n,k}), \quad (4.89)$$

and

$$\begin{aligned} \Delta_L^{n+1} |\rho_L^{n+1} - k| &\leq \Delta_L^n |\rho_L^n - k| + \mathfrak{h} |\rho_{m(n)-2}^n - k| \\ &\quad - \mathfrak{k} (Q_0^n - Q_{m(n)-2}^{-,n}) + \mathfrak{k} \mathbf{R}_L(k, \alpha_{n,\mathfrak{k}}) \end{aligned} \quad (4.90)$$

where $\bar{\rho}$ is defined at (3.65).

Proof. The inequality in (4.84) is classical and it is based on (3.55), (3.56).

The computations in the proofs of (4.85) - (4.90) being very similar, we only detail the inequalities involved in Case **B** to get (4.87) and (4.88). Remember that in this case $\rho_{m(n+1)-2}^{n+1}$ and ρ_L^{n+1} coincide, see (3.60), and their common value $\bar{\rho}$ is computed via (3.61).

Due to the monotonicity properties of the function H_L^{AB} and recalling (4.80), we have that

$$\begin{aligned} &H_L^{AB}(\rho_{m(n)-2}^n \wedge k, \rho_L^n \wedge k, \rho_R^n \wedge k; \mathfrak{k}, \Delta_L^n, \alpha_{n,\mathfrak{k}}) \\ &\leq H_L^{AB}(\rho_{m(n)-2}^n, \rho_L^n, \rho_R^n; \mathfrak{k}, \Delta_L^n, \alpha_{n,\mathfrak{k}}) \wedge H_L^{AB}(k, k, k; \mathfrak{k}, \Delta_L^n, \alpha_{n,\mathfrak{k}}) \\ &\leq \bar{\rho} \wedge k \end{aligned}$$

and similarly that

$$\bar{\rho} \vee k \leq H_L^{AB}(\rho_{m(n)-2}^n \vee k, \rho_L^n \vee k, \rho_R^n \vee k; \mathfrak{k}, \Delta_L^n, \alpha_{n,\mathfrak{k}}) + \frac{\mathfrak{k}}{\Delta_L^n + \alpha_{n,\mathfrak{k}} \mathfrak{k}} \mathbf{R}_L(k, \alpha_{n,\mathfrak{k}}).$$

Recalling (3.39),

$$\mathfrak{h} + \Delta_L^{n+1} = \Delta_L^n + \alpha_{n,\mathfrak{k}} \mathfrak{k}, \quad \Delta_R^{n+1} = \Delta_R^n - \alpha_{n,\mathfrak{k}} \mathfrak{k} + \mathfrak{h},$$

and the definition of H_L^{AB} in (4.68), we combine the previous inequalities to find that

$$\begin{aligned} (\mathfrak{h} + \Delta_L^{n+1}) |\bar{\rho} - k| &= (\mathfrak{h} + \Delta_L^{n+1}) [(\bar{\rho} \vee k) - (\bar{\rho} \wedge k)] \\ &\leq (\mathfrak{h} + \Delta_L^{n+1}) \left[H_L^{AB}(\rho_{m(n)-2}^n \vee k, \rho_L^n \vee k, \rho_R^n \vee k; \mathfrak{k}, \Delta_L^n, \alpha_{n,\mathfrak{k}}) \right. \\ &\quad \left. - H_L^{AB}(\rho_{m(n)-2}^n \wedge k, \rho_L^n \wedge k, \rho_R^n \wedge k; \mathfrak{k}, \Delta_L^n, \alpha_{n,\mathfrak{k}}) + \frac{\mathfrak{k}}{\Delta_L^n + \alpha_{n,\mathfrak{k}} \mathfrak{k}} \mathbf{R}_L(k, \alpha_{n,\mathfrak{k}}) \right] \\ &= \Delta_L^n [(\rho_L^n \vee k) - (\rho_L^n \wedge k)] \\ &\quad - \mathfrak{k} \left[h_0(\rho_L^n \vee k, \rho_R^n \vee k, \alpha_{n,\mathfrak{k}}) - h_0(\rho_L^n \wedge k, \rho_R^n \wedge k, \alpha_{n,\mathfrak{k}}) \right. \\ &\quad \left. - h^-(\rho_{m(n)-2}^n \vee k, \rho_L^n \vee k) + h^-(\rho_{m(n)-2}^n \wedge k, \rho_L^n \wedge k) \right] + \mathfrak{k} \mathbf{R}_L(k, \alpha_{n,\mathfrak{k}}) \\ &= \Delta_L^n |\rho_L^n - k| - \mathfrak{k} (Q_0^n - Q_{m(n)-1}^{-,n}) + \mathfrak{k} \mathbf{R}_L(k, \alpha_{n,\mathfrak{k}}). \end{aligned}$$

This proves (4.85). In a similar way

$$\begin{aligned} \rho_R^{n+1} \wedge k &\geq H_R^B(\rho_L^n \wedge k, \rho_R^n \wedge k, \rho_{m(n)+2}^n \wedge k, \rho_{m(n)+3}^n \wedge k; \mathfrak{k}, \mathfrak{h}, \Delta_R^n, \alpha_{n,\mathfrak{k}}), \\ \rho_R^{n+1} \vee k &\leq H_R^B(\rho_L^n \vee k, \rho_R^n \vee k, \rho_{m(n)+2}^n \vee k, \rho_{m(n)+3}^n \vee k; \mathfrak{k}, \mathfrak{h}, \Delta_R^n, \alpha_{n,\mathfrak{k}}) \end{aligned}$$

$$+ \frac{k}{\Delta_R^n + h - \alpha_{n,k} k} R_R(k, \alpha_{n,k}),$$

then

$$\begin{aligned} \Delta_R^{n+1} |\rho_R^{n+1} - k| &= \Delta_R^{n+1} [(\rho_R^{n+1} \vee k) - (\rho_R^{n+1} \wedge k)] \\ &\leq \Delta_R^{n+1} \left[H_R^B(\rho_L^n \vee k, \rho_R^n \vee k, \rho_{m(n)+2}^n \vee k, \rho_{m(n)+3}^n \vee k; k, h, \Delta_R^n, \alpha_{n,k}) \right. \\ &\quad \left. - H_R^B(\rho_L^n \wedge k, \rho_R^n \wedge k, \rho_{m(n)+2}^n \wedge k, \rho_{m(n)+3}^n \wedge k; k, h, \Delta_R^n, \alpha_{n,k}) \right. \\ &\quad \left. + \frac{k}{\Delta_R^n + h - \alpha_{n,k} k} R_R(k, \alpha_{n,k}) \right] \\ &= \Delta_R^n [(\rho_R^n \vee k) - (\rho_R^n \wedge k)] + h \left[(\rho_{m(n)+2}^n \vee k) - (\rho_{m(n)+2}^n \wedge k) \right] \\ &\quad - k \left[h^+(\rho_{m(n)+2}^n \vee k, \rho_{m(n)+3}^n \vee k) - h^+(\rho_{m(n)+2}^n \wedge k, \rho_{m(n)+3}^n \wedge k) \right] \\ &\quad - h_0(\rho_L^n \vee k, \rho_R^n \vee k, \alpha_{n,k}) + h_0(\rho_L^n \wedge k, \rho_R^n \wedge k, \alpha_{n,k}) + k R_R(k, \alpha_{n,k}) \\ &= \Delta_R^n |\rho_R^n - k| + h |\rho_{m(n)+2}^n - k| - k(Q_{m(n)+3}^{+,n} - Q_0^n) + k R_R(k, \alpha_{n,k}). \end{aligned}$$

This completes the proof of (4.86). \square

Next, we define the approximate entropy flux $Q^h(x, t)$ as follows:

$$\begin{aligned} Q^h(x, t) &= \sum_n \left[\sum_{j \leq m(n)-1} Q_j^{-,n} \cdot \mathbb{1}_{P_{j-1}^n}(x, t) + Q_0^n \cdot \mathbb{1}_{P_{m(n)-1}^n}(x, t) + \sum_{j \geq m(n)+1} Q_{j+1}^{+,n} \cdot \mathbb{1}_{P_j^n}(x, t) \right], \end{aligned}$$

where, using (3.28) and Definition 3.1, we set

$$\begin{aligned} P_j^n &:= C_j \times [t^n, t^{n+1}), \quad j \neq m(n), m(n) \pm 1 \\ P_L^n &:= \{(x, t) : x_{m(n)-3/2} \leq x < \xi^k(t), t^n \leq t < t^{n+1}\} \\ P_R^n &:= \{(x, t) : \xi^k(t) < x \leq x_{m(n)+3/2}, t^n \leq t < t^{n+1}\}. \end{aligned}$$

Otherwise written as

$$Q^h(x, t) = \begin{cases} Q_{j+1}^{-,n} & (x, t) \in P_j^n, \quad j \leq m(n) - 2 \\ Q_0^n & (x, t) \in P_L^n \\ Q_{j+1}^{+,n} & (x, t) \in P_j^n, \quad j \geq m(n) + 1 \end{cases}$$

Proposition 4.2. (Approximate entropy inequalities). Fix $n \in \mathbb{N}$, $k \in [0, 1]$ and let $\varphi \in C_c^\infty([0, T] \times \mathbb{R})$, with $\varphi \geq 0$. There holds

$$\begin{aligned} &\int_{t^n}^{t^{n+1}} \int_{\mathbb{R}} (|\rho^h - k| \partial_t \varphi + Q^\Delta(\rho^h, k) \partial_x \varphi) dx dt + \\ &+ \int_{\mathbb{R}} |\rho^h(t^n, x) - k| \varphi(t^n, x) dx - \int_{\mathbb{R}} |\rho^h(t^{n+1}, x) - k| \varphi(t^{n+1}, x) dx \end{aligned}$$

$$+ \int_{t^n}^{t^{n+1}} 2f(k)\varphi(t, \xi^k(t)) dx \geq \mathcal{O}(h^2) + \mathcal{O}(hk) + \mathcal{O}(k^2).$$

Proof. For any $n \in \mathbb{N}$, we can define a piecewise constant discretization of the profile of test function φ at time $t = t^n$

$$\varphi(t^n, x) \approx \sum_{j \neq m(n)} \varphi_j^n \mathbb{1}_{C_j^n}(x) = \sum_{j \neq m(n)} \mathbb{1}_{C_j^n}(x) \frac{1}{|C_j^n|} \int_{C_j^n} \varphi(t^n, x) dx.$$

Recalling the notation (3.34) for Δ_L^n and Δ_R^n , we consider

$$\begin{aligned} \varphi_{\Delta_R^n}^{n+1} &= \frac{1}{\Delta_R^n} \int_{D_R^n} \varphi(t^{n+1}, x) dx, & \varphi_{\Delta_L^n}^{n+1} &= \frac{1}{\Delta_L^n} \int_{D_L^n} \varphi(t^{n+1}, x) dx, \\ \varphi_{\Delta_\xi^n}^{n+1} &= \frac{1}{\alpha_{n,k} k} \int_{\xi^n}^{\xi^{n+1}} \varphi(t^{n+1}, x) dx & \varphi_{m(n)+2}^{n+1} &= \frac{1}{h} \int_{x_{m(n)+3/2}}^{x_{m(n)+5/2}} \varphi(t^{n+1}, x) dx. \end{aligned}$$

The following computations apply to Case B, that is, $m(n+1) = m(n) + 1$. We multiply each of the discrete entropy inequalities in (4.84), (4.87) and (4.88) by φ_j^{n+1} , for $j \neq m(n+1)$ and we sum them to obtain

$$\begin{aligned} & \sum_{j \neq m(n+1)} |C_j^{n+1}| |\rho_j^{n+1} - k| \varphi_j^{n+1} \\ & \leq \sum_{j \leq m(n+1)-3} [|C_j^n| |\rho_j^n - k| - k(Q_{j+1}^{-,n} - Q_j^{-,n})] \varphi_j^{n+1} \\ & + \sum_{j \geq m(n+1)-2} [|C_j^n| |\rho_j^n - k| - k(Q_{j+1}^{+,n} - Q_j^{+,n})] \varphi_j^{n+1} \\ & + [\Delta_L^n |\rho_L^n - k| - k(Q_0^n - Q_{m(n)-1}^{-,n}) + kR_L(k, \alpha_{n,k})] \varphi_{m(n+1)-1}^{n+1} \\ & + h|\bar{\rho} - k| (\varphi_{m(n+1)-2}^{n+1} - \varphi_{m(n+1)-1}^{n+1}) \\ & + [\Delta_R^n |\rho_R^n - k| + h|\rho_{m(n)+2}^n - k| - k(Q_{m(n)+3}^{+,n} - Q_0^n) + kR_R(k, \alpha_{n,k})] \varphi_{m(n+1)+1}^{n+1}. \end{aligned} \tag{4.91}$$

Thanks to equality (3.39) and the fact that $|\Delta_L^p| + |\Delta_R^p| = 3h$, for any p , we observe that

$$\begin{aligned} \Delta_R^n |\rho_R^n - k| \varphi_{m(n+1)+1}^{n+1} &= \Delta_R^n |\rho_R^n - k| \frac{1}{\Delta_{R^{n+1}}} \int_{\Delta_{R^{n+1}}} \varphi(t^{n+1}, x) dx \\ &= \Delta_R^n |\rho_R^n - k| \frac{1}{\Delta_{R^{n+1}}} \left[|\Delta_R^n| \frac{1}{|\Delta_R^n|} \int_{\Delta_R^n} \varphi(t^{n+1}, x) dx + h \frac{1}{h} \int_{x_{m(n+1)+1/2}}^{x_{m(n+1)+3/2}} \varphi(t^{n+1}, x) dx \right. \\ & \quad \left. - \alpha_{n,k} k \frac{1}{\alpha_{n,k} k} \int_{\xi^n}^{\xi^{n+1}} \varphi(t^{n+1}, x) dx \right] \\ &= \Delta_R^n |\rho_R^n - k| \frac{1}{\Delta_{R^{n+1}}} \left[|\Delta_R^n| \varphi_{\Delta_R^n}^{n+1} + h \varphi_{m(n)+2}^{n+1} - \alpha_{n,k} k \varphi_{\Delta_\xi^n}^{n+1} \right] \\ &= \Delta_R^n |\rho_R^n - k| \varphi_{\Delta_R^n}^{n+1} + \Delta_R^n |\rho_R^n - k| \left[-\frac{\Delta_R^{n+1} - |\Delta_R^n|}{\Delta_{R^{n+1}}} \varphi_{\Delta_R^n}^{n+1} + \frac{h}{\Delta_{R^{n+1}}} \varphi_{m(n)+2}^{n+1} - \frac{\alpha_{n,k} k}{\Delta_{R^{n+1}}} \varphi_{\Delta_\xi^n}^{n+1} \right] \end{aligned}$$

$$\begin{aligned}
&= \Delta_R^n |\rho_R^n - k| \varphi_{\Delta_R^n}^{n+1} + \Delta_R^n |\rho_R^n - k| \left[\frac{\mathbf{h}}{\Delta_R^{n+1}} \left(\varphi_{m(n)+2}^{n+1} - \varphi_{\Delta_R^n}^{n+1} \right) - \frac{\alpha_{n,k} \mathbf{k}}{\Delta_R^{n+1}} \left(\varphi_{\Delta_\xi}^{n+1} - \varphi_{\Delta_R^n}^{n+1} \right) \right] \\
&= \Delta_R^n |\rho_R^n - k| \varphi_{\Delta_R^n}^{n+1} + (\mathcal{O}(\mathbf{h}^2) + \mathcal{O}(\mathbf{hk})) \|\rho_0\|_\infty \|\partial_x \varphi\|_\infty,
\end{aligned}$$

and, recalling that $|C_{m(n)+2}^n| = \mathbf{h}$

$$\begin{aligned}
|C_{m(n)+2}^n| |\rho_{m(n)+2}^n - k| \varphi_{m(n)+1}^{n+1} &= |C_{m(n)+2}^n| |\rho_{m(n)+2}^n - k| \varphi_{m(n)+2}^{n+1} \\
&\quad + |C_{m(n)-2}^n| |\rho_{m(n)+2}^n - k| \left[\frac{|\Delta_R^n|}{\Delta_R^{n+1}} \left(\varphi_{m(n)+2}^{n+1} - \varphi_{\Delta_R^n}^{n+1} \right) - \frac{\alpha_{n,k} \mathbf{k}}{\Delta_R^{n+1}} \left(\varphi_{m(n)+2}^{n+1} - \varphi_{\Delta_\xi}^{n+1} \right) \right] \\
&= |C_{m(n)+2}^n| |\rho_{m(n)+2}^n - k| \varphi_{m(n)+2}^{n+1} + (\mathcal{O}(\mathbf{h}^2) + \mathcal{O}(\mathbf{hk})) \|\rho_0\|_\infty \|\partial_x \varphi\|_\infty,
\end{aligned}$$

On the left side of the interface, we similarly have,

$$\begin{aligned}
\Delta_L^n |\rho_L^n - k| \varphi_{m(n)+1}^{n+1} &= \Delta_L^n |\rho_L^n - k| \frac{1}{\Delta_L^{n+1}} \int_{\Delta_R^{n+1}} \varphi(t^{n+1}, x) dx \\
&= \Delta_L^n |\rho_L^n - k| \frac{1}{\Delta_L^{n+1}} \left[|\Delta_L^n| \varphi_{\Delta_L^n}^{n+1} - \mathbf{h} \varphi_{m(n)+2}^{n+1} + \alpha_{n,k} \mathbf{k} \varphi_{\Delta_\xi}^{n+1} \right] \\
&= \Delta_L^n |\rho_L^n - k| \varphi_{\Delta_L^n}^{n+1} + \Delta_L^n |\rho_L^n - k| \left[\frac{\mathbf{h}}{\Delta_L^{n+1}} \left(\varphi_{m(n)+2}^{n+1} - \varphi_{\Delta_L^n}^{n+1} \right) - \frac{\alpha_{n,k} \mathbf{k}}{\Delta_L^{n+1}} \left(\varphi_{\Delta_\xi}^{n+1} - \varphi_{\Delta_L^n}^{n+1} \right) \right] \\
&= \Delta_L^n |\rho_L^n - k| \varphi_{\Delta_L^n}^{n+1} + (\mathcal{O}(\mathbf{h}^2) + \mathcal{O}(\mathbf{hk})) \|\rho_0\|_\infty \|\partial_x \varphi\|_\infty.
\end{aligned}$$

In the notation of Def. 3.1, we recall that $C_j^n = C_j^{n+1}$ for all $j \leq m(n+1) - 3 = m(n) - 2$ or $j \geq m(n+1) + 2 = m(n) + 3$ and that $C_{m(n)-1}^n = D_L^n$, $C_{m(n)+1}^n = D_R^n$. With these notations, the estimates above and classical rearranging of the terms in (4.91) allow us to write

$$\begin{aligned}
&\sum_{j \neq m(n+1)} |C_j^{n+1}| |\rho_j^{n+1} - k| \varphi_j^{n+1} - \sum_{j \neq m(n)-1, m(n), m(n)+1} |C_j^n| |\rho_j^n - k| \varphi_j^{n+1} \\
&\quad - |\Delta_L^n| |\rho_L^n - k| \varphi_{\Delta_L^n}^{n+1} - |\Delta_R^n| |\rho_R^n - k| \varphi_{\Delta_R^n}^{n+1} \\
&\leq -k \left[\sum_{j \leq m(n+1)-3} Q_j^{-,n} (\varphi_{j-1}^{n+1} - \varphi_j^{n+1}) + \sum_{j \geq m(n+1)+3} Q_j^{+,n} (\varphi_{j-1}^{n+1} - \varphi_j^{n+1}) \right] \\
&\quad - k \left[Q_{m(n)-1}^{-,n} \varphi_{m(n)+3}^{n+1} - Q_{m(n)+3}^{+,n} \varphi_{m(n)+2}^{n+1} \right] \\
&\quad + \left(Q_0^n - Q_{m(n)-1}^{-,n} \right) \varphi_{m(n)+1}^{n+1} + \left(Q_{m(n)+3}^{+,n} - Q_0^n \right) \varphi_{m(n)+1}^{n+1} \\
&\quad + k \left[\mathbf{R}_L(k, \alpha_{n,k}) \varphi_{m(n)+1}^{n+1} + \mathbf{R}_R(k, \alpha_{n,k}) \varphi_{m(n)+1}^{n+1} \right] \\
&\quad + \mathbf{h} |\bar{\rho} - k| \left(\varphi_{m(n)+2}^{n+1} - \varphi_{m(n)+1}^{n+1} \right) + (\mathcal{O}(\mathbf{h}^2) + \mathcal{O}(\mathbf{hk})) \|\rho_0\|_\infty \|\partial_x \varphi\|_\infty \\
&\leq -k \left[\sum_{j \leq m(n+1)-2} Q_j^{-,n} (\varphi_{j-1}^{n+1} - \varphi_j^{n+1}) + \sum_{j \geq m(n+1)+2} Q_j^{+,n} (\varphi_{j-1}^{n+1} - \varphi_j^{n+1}) \right] \\
&\quad - k \left[Q_0^n \left(\varphi_{m(n)+1}^{n+1} - \varphi_{m(n)+1}^{n+1} \right) + Q_{m(n)-1}^{-,n} \left(\varphi_{m(n)+2}^{n+1} - \varphi_{m(n)+1}^{n+1} \right) \right. \\
&\quad \quad \left. + Q_{m(n)+3}^{+,n} \left(\varphi_{m(n)+1}^{n+1} - \varphi_{m(n)+2}^{n+1} \right) \right]
\end{aligned}$$

$$\begin{aligned}
& + k \left[(\mathbf{R}_L(k, \alpha_{n,k}) + \mathbf{R}_R(k, \alpha_{n,k})) \varphi_{m(n+1)-1}^{n+1} + \mathbf{R}_R(k, \alpha_{n,k}) \left(\varphi_{m(n+1)+1}^{n+1} - \varphi_{m(n+1)-1}^{n+1} \right) \right] \\
& + h|\bar{\rho} - k| \left(\varphi_{m(n+1)-2}^{n+1} - \varphi_{m(n+1)-1}^{n+1} \right) + (\mathcal{O}(h^2) + \mathcal{O}(hk)) \|\rho_0\|_\infty \|\partial_x \varphi\|_\infty. \quad (4.92)
\end{aligned}$$

We can easily estimate some of the terms above

$$kQ_0^n \left(\varphi_{m(n+1)-1}^{n+1} - \varphi_{m(n+1)+1}^{n+1} \right) \leq 8kh \|f\|_\infty \|\partial_x \varphi\|_\infty; \quad (4.93)$$

$$kQ_{m(n)-1}^{-,n} \left(\varphi_{m(n+1)-2}^{n+1} - \varphi_{m(n+1)-1}^{n+1} \right) \leq 4kh \|f\|_\infty \|\partial_x \varphi\|_\infty; \quad (4.94)$$

$$kQ_{m(n)+3}^{+,n} \left(\varphi_{m(n+1)+1}^{n+1} - \varphi_{m(n+1)+2}^{n+1} \right) \leq 4kh \|f\|_\infty \|\partial_x \varphi\|_\infty; \quad (4.95)$$

$$k\mathbf{R}_R(k, \alpha_{n,k}) \left(\varphi_{m(n+1)+1}^{n+1} - \varphi_{m(n+1)-1}^{n+1} \right) \leq 8kh \|f\|_\infty \|\partial_x \varphi\|_\infty; \quad (4.96)$$

$$h|\bar{\rho} - k| \left(\varphi_{m(n+1)-2}^{n+1} - \varphi_{m(n+1)-1}^{n+1} \right) \leq 2h^2 \|\rho_0\|_\infty \|\partial_x \varphi\|_\infty. \quad (4.97)$$

Recalling that $\mathbf{R}_L(k, \alpha_{n,k}) + \mathbf{R}_R(k, \alpha_{n,k}) = 2f(k)$, and using the estimates above we get

$$\sum_{j \neq m(n+1)} |\mathbf{C}_j^{n+1}| |\rho_j^{n+1} - k| \varphi_j^{n+1} \quad (4.98)$$

$$- \sum_{j \neq m(n), m(n) \pm 1} |\mathbf{C}_j^n| |\rho_j^n - k| \varphi_j^{n+1} - \Delta_L^n |\rho_L^n - k| \varphi_{\Delta_L^n}^{n+1} - \Delta_R^n |\rho_R^n - k| \varphi_{\Delta_R^n}^{n+1} \quad (4.99)$$

$$\leq -k \left[\sum_{j \leq m(n+1)-2} Q_j^{-,n} (\varphi_{j-1}^{n+1} - \varphi_j^{n+1}) + \sum_{j \geq m(n+1)+2} Q_j^{+,n} (\varphi_{j-1}^{n+1} - \varphi_j^{n+1}) \right] \quad (4.100)$$

$$+ 2kf(k) \varphi_{m(n+1)-1}^{n+1} + \mathcal{O}(h^2) + \mathcal{O}(hk). \quad (4.101)$$

To which we add and subtract the terms

$$\sum_{j \neq m(n), m(n) \pm 1} |\mathbf{C}_j^n| |\rho_j^n - k| \varphi_j^n + \Delta_L^n |\rho_L^n - k| \varphi_{\Delta_L^n}^n + \Delta_R^n |\rho_R^n - k| \varphi_{\Delta_R^n}^n,$$

which can also be written as $\sum_{j \neq m(n)} |\mathbf{C}_j^n| |\rho_j^n - k| \varphi_j^n$, so that lines (4.98), (4.99) become

$$\begin{aligned}
& \sum_{j \neq m(n+1)} |\mathbf{C}_j^{n+1}| |\rho_j^{n+1} - k| \varphi_j^{n+1} - \sum_{j \neq m(n)} |\mathbf{C}_j^n| |\rho_j^n - k| \varphi_j^n \\
& - \sum_{j \neq m(n)-1, m(n), m(n)+1} |\mathbf{C}_j^n| |\rho_j^n - k| (\varphi_j^{n+1} - \varphi_j^n) \\
& - \Delta_L^n |\rho_L^n - k| (\varphi_{\Delta_L^n}^{n+1} - \varphi_{\Delta_L^n}^n) - \Delta_R^n |\rho_R^n - k| (\varphi_{\Delta_R^n}^{n+1} - \varphi_{\Delta_R^n}^n).
\end{aligned}$$

□

5 Numerical Examples and Validation

We conclude the article by examining the performance and accuracy of the proposed numerical scheme applied to selected examples compared to the standard Godunov scheme without any moving mesh adaptation.

5.1 Examples

To observe the changes in the slope of the interface and its interactions with classical waves, two examples are chosen.

Let $f(\rho) = \rho(1 - \rho)$ and consider the turning curve,

$$\xi(t) := \xi_0 + \int_0^t \xi'(s) ds,$$

with $\xi_0 = -0.1$ and the following sets of initial data and slope of the discontinuity :

	Initial data	slope of the discontinuity
A :	$\rho_0(x) = \begin{cases} 3/5, & \text{if } -1 < x < 3/10 \\ 9/10, & \text{if } 3/10 \leq x < 1. \end{cases}$	$\xi'(s) = \begin{cases} 2/5, & \text{for } 0 < s < 3/5 \\ 0, & \text{for } s \geq 3/5 \end{cases}$
B :	$\rho_0(x) = \begin{cases} 9/10, & \text{if } -1/10 \leq x \leq 1/2 \\ 3/5, & \text{if otherwise.} \end{cases}$	$\xi'(s) = \begin{cases} 1/10, & \text{for } 0 < s \leq 3/10, \\ 1/4, & \text{for } 3/10 < s \leq 3/5, \\ 0, & \text{for } s > 3/5. \end{cases}$

The exact solutions are constructed using the method of characteristics. As $\rho(0, x) > 1/2$, the boundary conditions require that rarefaction waves enter the boundary points $\{(t, -1^+)\}$ and $\{(t, 1^-)\}$ such that $\rho(t, \pm 1) \geq 1/2$ for all $t > 0$.

Example **A**: For $0 < t \leq 4/9$, two undercompressive shocks, $\sigma_L(t) = -1/10(1 + 4t)$ and $\sigma_R(t) = -1/10(1 - 4t)$, separated by vacuum, are generated at $x = \xi(0)$, while at $x = 0.3$, a single shock $\sigma_1(t) = 0.3 - 0.5t$ is also created. Observing that $\xi(t) = \sigma_R(t)$ and since $\dot{\sigma}_L > \dot{\sigma}_1$, the interface interacts with the shock σ_1 at $t = 4/9$. The solution for $t \in [0, 4/9)$ writes,

$$\rho(t, x) = \begin{cases} 0.6 & \text{if } -1 < x < \sigma_L(t) \\ 0 & \text{if } -\sigma_L(t) \leq x < \xi(t) \\ 0.6 & \text{if } \xi(t) \leq x < \sigma_R(t) \\ 0.9 & \text{if } \sigma_R(t) \leq x < 1. \end{cases}$$

At $t = 4/9$, a slight decrease in density is observed and a solution to the Riemann problem at ξ is calculated with an intermediate state $\rho_M = 1/10 \left(7 - 1/2 \sqrt{\frac{88}{10}} \right)$ for the time period between

4/9 and 6/10. The solution in this time frame is as follows:

$$\rho(t, x) = \begin{cases} 0.6 & \text{if } -1 < x < \sigma_L(t), \\ 0 & \text{if } -\sigma_L(t) \leq x < 7/90 - (t - 4/9), \\ \frac{x-7/90}{2(t-4/9)} + \frac{1}{2} & \text{if } 7/90 - (t - 4/9) \leq x < 7/90 - \dot{R}_{\max}(t - 4/9), \\ \rho_M & \text{if } 7/90 - \dot{R}_{\max}(t - 4/9) \leq x < \xi(t), \\ 0.9 & \text{if } \xi \leq x < 1. \end{cases}$$

Here $\dot{R}_{\max} = 1/5 \left(2 - 1/2\sqrt{\frac{88}{10}} \right)$, denotes the maximum slope of the rarefaction fan.

Example **B**: At $x = 0.5$, a rarefaction is formed with a value of $1/2 + f'(\rho)t$, where ρ is in the range of $[0.6, 0.9]$. Additionally, two shocks are created, $\sigma_L(t) = -0.1 + 0.4t$ and $\sigma_R = -0.1 + 0.1t$, which originate from $\xi(0) = -0.1$ for $0 < t \leq 3/10$. The solution is as follows

$$\rho(t, x) = \begin{cases} 6/10 & \text{if } -1 + 8t/10 \leq x \leq \sigma_L(t), \\ 0 & \text{if } \sigma_L(t) < x < \xi(t), \\ 0.9 & \text{if } \xi(t) < x \leq R_{\min}^0(t), \\ (t-x)/2t & \text{if } \dot{R}_{\min}^0(t) < (x-1/2)/t \leq \dot{R}_{\max}^0(t), \\ 6/10, & \text{if } 1/2(1-t/5) < x < 1 - 8t/10, \end{cases}$$

where \dot{R}_{\min}^0 and \dot{R}_{\max}^0 represents the minimum and maximum speeds of the R^0 . For $3/10 \leq t \leq 6/10$, the solution writes

$$\rho(t, x) = \begin{cases} 6/10 & \text{if } -1 + 8t/10 \leq x \leq \sigma_L(t), \\ 0 & \text{if } \sigma_L(t) < x < R_{\min}^1(t), \\ \frac{1}{2} + \frac{x+1/40}{2(t-3/10)}, & \text{if } \dot{R}_{\min}^1(t) \leq x \leq \dot{R}^1(t) \\ \rho_M, & \text{if } R_{\max}^1(t) \leq x < \xi(t) \\ 9/10, & \text{if } \xi(t) \leq x < R_{\min}^0(t) \\ (t-x)/2t & \text{if } \dot{R}_{\min}^0(t) < (x-1/2)/t \leq \dot{R}_{\max}^0(t), \\ 6/10 & R_{\max}^0(t) \leq x < 1 - 8t/10, \end{cases}$$

by noting that a Riemann problem at ξ is solved with an intermediate state of $\rho_M = \frac{1}{80}(50 - \sqrt{1636})$ and a small rarefaction denoted $R^1(t) = -\frac{1}{40} - f'(\rho) \left(t - \frac{3}{10} \right)$ for $\rho \in [0, \rho_M]$ when it interacts with the shock σ_R . This occurs for $3/10 \leq t < 6/10$. The approximate solutions of these two examples are depicted in the $x-t$ can be found in Figure 4. However, we exclusively display the simulation results of Example **A** at selected times in Figure 5. To illustrate the effectiveness of the scheme in handling discontinuities with negative slopes, particularly during wave interactions with ξ , we present in Figure 6 the simulation results of a third example, denoted as Example **C**, where the initial density ρ_0 is defined as in Example **A**. However, the slope of

the flux interface is specified as follows:

$$\xi'(s) = \begin{cases} 1/10, & \text{for } 0 < s \leq 3/10, \\ 1/4, & \text{for } 3/10 < s \leq 6/10, \\ -3/2, & \text{for } 6/10 < s \leq 1, \\ 0, & \text{for } s > 1. \end{cases} \quad (5.102)$$

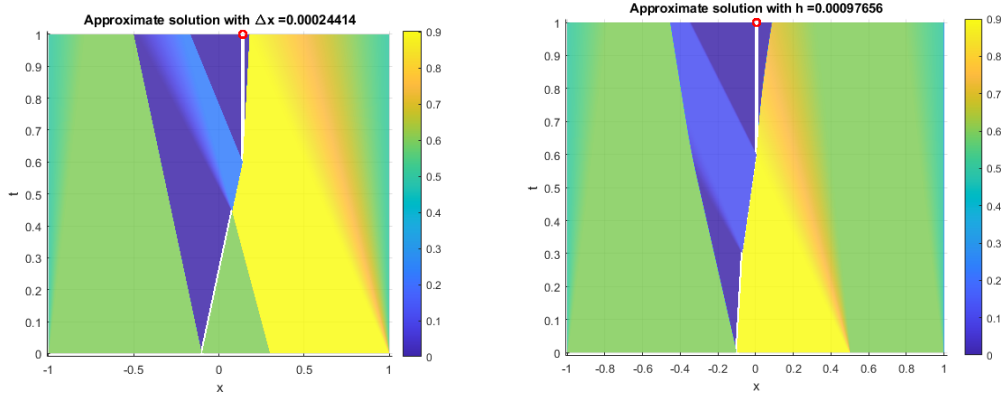


Fig. 4 Approximate solution of Examples **A** (left) and **B** (right) in the $x - t$ plane.

5.2 Order of convergence

In this section, we assess the accuracy of the numerical scheme we proposed by estimating the \mathbf{L}^1 errors and deducing the order of convergence on Examples **A** and **B**. These examples are carefully chosen to enable us to observe the performance of our scheme during collisions between the turning curve and incoming waves. The numerical \mathbf{L}^1 -norm at time level $n = T/k$ writes

$$Err(n, h) = \sum_{j \neq m(n), |j| \leq \frac{1}{h}} |\rho(T, x_j^n) - \rho_j^n| h, \quad (5.103)$$

where $\rho(T, x)$ is the exact solution which we use as the reference solution and ρ_j^n is the approximate solution obtained with our scheme. In these simulations, we use a CFL number of 0.45, and plot the log-log graph of the errors against N values for Examples A and B below at times where the interface collides with the incoming waves. We first show the graph of the approximate solution in the $x - t$ plane for examples A and B.

We analyze the performance of our scheme with the standard Godunov flux by comparing Example A at $T = 0.55$, where a collision is seen in figure 7. The figure shows that the standard Godunov flux produces spurious oscillations at $x = \xi(t)$ when a shock wave from the right interacts with ξ . In contrast, the modified scheme not only eliminates these oscillations, but also accurately captures the non-zero intermediate state that is formed after the interaction.

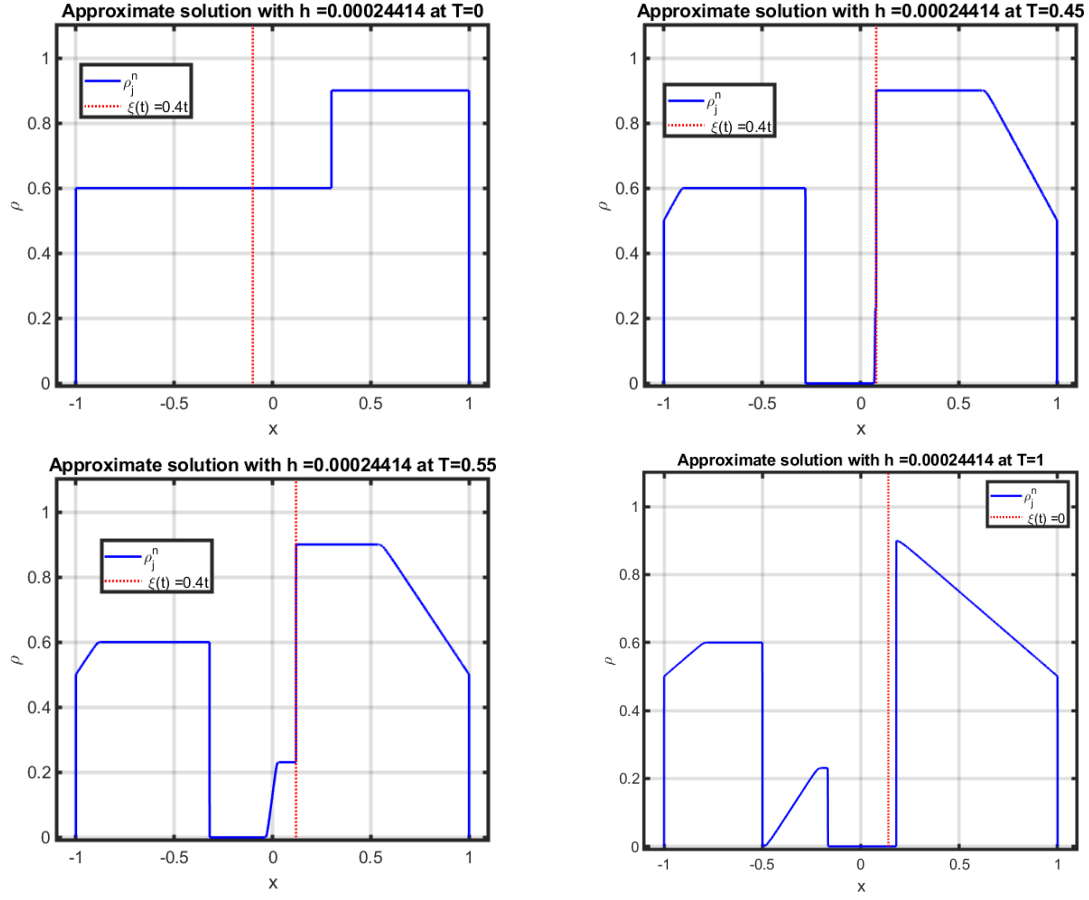


Fig. 5 Evolution of the approximate solution of Examples **A** in the $\rho - x$ plane for $t = 0, 0.45, 0.55,$ and 1.0 .

h	Example A		Example B	
	$Err(h)$	$\frac{\ln(Err(h))}{\ln(h)}$	$Err(h)$	$\frac{\ln(Err(h))}{\ln(h)}$
$1.5625e-02$	$3.4222e-02$	-0.79	$7.5633e-3$	-0.79
$3.9062e-03$	$1.0174e-02$	-0.80	$4.2297e-3$	-0.79
$9.7656e-04$	$3.1818e-03$	-0.81	$3.1088e-3$	-0.79
$4.8828e-04$	$1.7271e-03$	-0.81	$2.4516e-3$	-0.79
$2.4414e-04$	$9.7091e-04$	-0.81	$1.8074e-3$	-0.79
$1.2207e-04$	$5.2053e-04$	-0.81	$1.2818e-3$	-0.78

Table 1 L^1 -errors at $T = 0.55$, for example A and at $T = 0.58$ for example B with mesh size from $h = 1/500, \dots, 1/5000$.

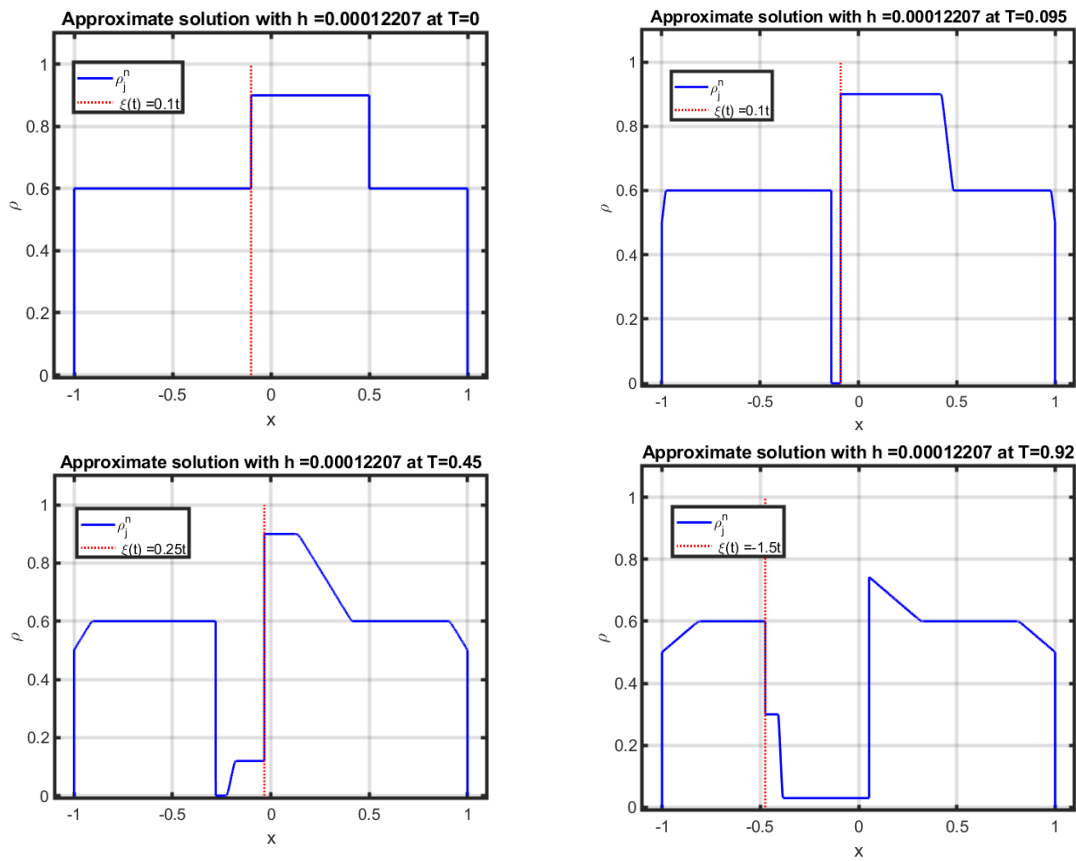


Fig. 6 Evolution of the approximate solution of Examples **C** in the $\rho - x$ plane for $t = 0, 0.095, 0.45,$ and 0.92 .

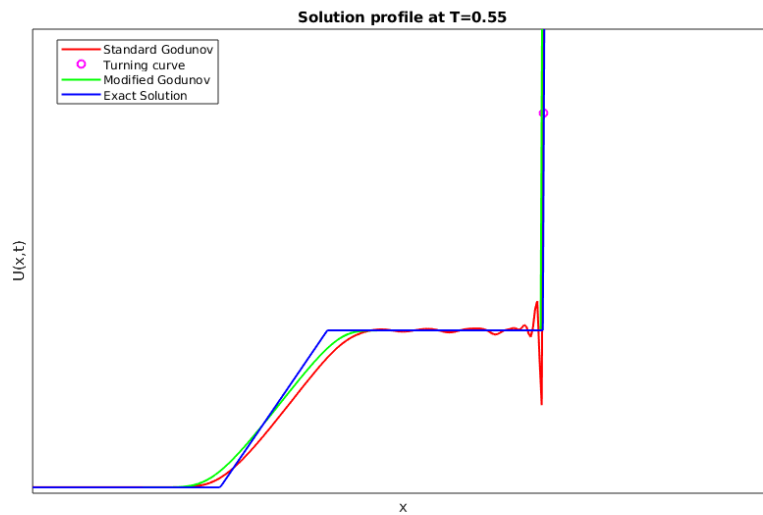


Fig. 7 A zoomed view of exact solution and the numerical solutions with the standard Godunov's flux and the modified flux at $T = 0.55$. The violet circle represents the position of the interface.

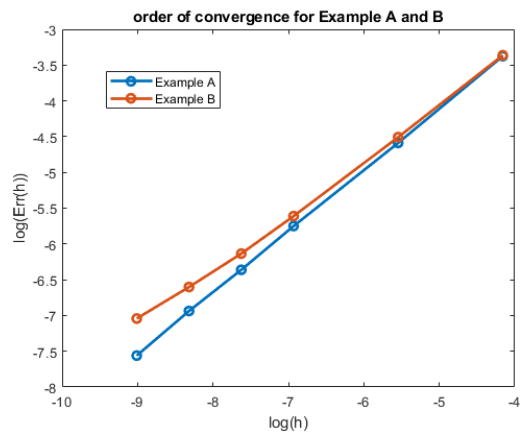


Fig. 8 The log-log graph of L^1 error against h on Example A and B at $T = 0.55$ and $T = 0.58$ respectively.

References

- [1] Adimurthi, Jérôme Jaffré, and GD Veerappa Gowda. “Godunov-type methods for conservation laws with a flux function discontinuous in space”. In: *SIAM Journal on Numerical Analysis* 42.1 (2004), pp. 179–208.
- [2] Adimurthi, Siddhartha Mishra, and GD Veerappa Gowda. “Optimal entropy solutions for conservation laws with discontinuous flux-functions”. In: *Journal of Hyperbolic Differential Equations* 2.04 (2005), pp. 783–837.
- [3] Debora Amadori and Marco Di Francesco. “The one-dimensional hughes model for pedestrian flow: Riemann—type solutions”. In: *Acta Mathematica Scientia* 32.1 (2012), pp. 259–280.
- [4] Debora Amadori, Paola Goatin, and Massimiliano D Rosini. “Existence results for Hughes’ model for pedestrian flows”. In: *Journal of Mathematical Analysis and applications* 420.1 (2014), pp. 387–406.
- [5] Boris Andreianov and Clément Cancès. “On interface transmission conditions for conservation laws with discontinuous flux of general shape”. In: *Journal of hyperbolic differential equations* 12.02 (2015), pp. 343–384.
- [6] Boris Andreianov and Clément Cancès. “The Godunov scheme for scalar conservation laws with discontinuous bell-shaped flux functions”. In: *Applied Mathematics Letters* 25.11 (2012), pp. 1844–1848.
- [7] Boris Andreianov, Paola Goatin, and Nicolas Seguin. “Finite volume schemes for locally constrained conservation laws”. In: *Numerische Mathematik* 115 (2010), pp. 609–645.
- [8] Boris Andreianov, Kenneth Hvistendahl Karlsen, and Nils Henrik Risebro. “A theory of L^1 -dissipative solvers for scalar conservation laws with discontinuous flux”. In: *Archive for rational mechanics and analysis* 201 (2011), pp. 27–86.
- [9] Boris Andreianov and Abraham Sylla. “Finite volume approximation and well-posedness of conservation laws with moving interfaces under abstract coupling conditions”. In: *Nonlinear Differential Equations and Applications NoDEA* 30.4 (2023), p. 53.
- [10] Florence Bachmann. “Finite volume schemes for a nonlinear hyperbolic conservation law with a flux function involving discontinuous coefficients”. In: *International Journal on Finite Volumes* 3.1 (2006), pp. 1–38.
- [11] Claude Bardos, Alain-Yves LeRoux, and Jean-Claude Nédélec. “First order quasilinear equations with boundary conditions”. In: *Communications in partial differential equations* 4.9 (1979), pp. 1017–1034.
- [12] Raimund Bürger and Kenneth H Karlsen. “On a diffusively corrected kinematic-wave traffic flow model with changing road surface conditions”. In: *Mathematical Models and Methods in Applied Sciences* 13.12 (2003), pp. 1767–1799.
- [13] Raimund Bürger et al. “Well-posedness in BV t and convergence of a difference scheme for continuous sedimentation in ideal clarifier-thickener units”. In: *Numerische Mathematik* 97 (2004), pp. 25–65.
- [14] Christophe Chalons, Maria Laura Delle Monache, and Paola Goatin. “A conservative scheme for non-classical solutions to a strongly coupled PDE-ODE problem”. In: *Interfaces and Free Boundaries* 19.4 (2018), pp. 553–570.
- [15] Giuseppe Maria Coclite and Nils Henrik Risebro. “Conservation laws with time dependent discontinuous coefficients”. In: *SIAM journal on mathematical analysis* 36.4 (2005), pp. 1293–1309.

- [16] Rinaldo M Colombo and Paola Goatin. “A well posed conservation law with a variable unilateral constraint”. In: *Journal of Differential Equations* 234.2 (2007), pp. 654–675.
- [17] Maria Laura Delle Monache and Paola Goatin. “A front tracking method for a strongly coupled PDE-ODE system with moving density constraints in traffic flow”. In: *Discrete and Continuous Dynamical Systems-Series S* 7.3 (2014), pp. 435–447.
- [18] Maria Laura Delle Monache and Paola Goatin. “A numerical scheme for moving bottlenecks in traffic flow”. In: *Bulletin of the Brazilian Mathematical Society, New Series* 47 (2016), pp. 605–617.
- [19] Stefan Diehl. “On scalar conservation laws with point source and discontinuous flux function”. In: *SIAM journal on mathematical analysis* 26.6 (1995), pp. 1425–1451.
- [20] Sylvain Dotti and Julien Vovelle. “Convergence of the Finite Volume Method for scalar conservation laws with multiplicative noise: an approach by kinetic formulation”. In: *Stochastics and Partial Differential Equations: Analysis and Computations* 2.8 (2019), pp. 1–46.
- [21] Rajib Dutta, GD Veerappa Gowda, Jérôme Jaffré, et al. “Monotone (A, B) entropy stable numerical scheme for scalar conservation laws with discontinuous flux”. In: *ESAIM: Mathematical Modelling and Numerical Analysis* 48.6 (2014), pp. 1725–1755.
- [22] Lawrence C Evans. “”Partial Differential Equations,””. In: *Graduate Studies in Mathematics* (1998).
- [23] R Eymard et al. “Analysis tools for finite volume schemes”. In: *Proceedings of Equadiff 11* (2007), pp. 111–136.
- [24] Robert Eymard, Thierry Gallouët, and Raphaële Herbin. “Finite volume methods”. In: *Handbook of numerical analysis* 7 (2000), pp. 713–1018.
- [25] Tore Gimse and Nils Henrik Risebro. “Solution of the Cauchy problem for a conservation law with a discontinuous flux function”. In: *SIAM Journal on Mathematical Analysis* 23.3 (1992), pp. 635–648.
- [26] Paola Goatin and Matthias Mimault. “The wave-front tracking algorithm for Hughes’ model of pedestrian motion”. In: *SIAM Journal on Scientific Computing* 35.3 (2013), B606–B622.
- [27] Roger L Hughes. “A continuum theory for the flow of pedestrians”. In: *Transportation Research Part B: Methodological* 36.6 (2002), pp. 507–535.
- [28] Jérôme Jaffré. “Flux calculation at the interface between two rock types for two-phase flow in porous media”. In: *Transport in Porous media* 21 (1995), pp. 195–207.
- [29] Kenneth H Karlsen and John D Towers. “Convergence of the Lax-Friedrichs scheme and stability for conservation laws with a discontinuous space-time dependent flux”. In: *Chinese Annals of Mathematics* 25.03 (2004), pp. 287–318.
- [30] Kenneth Hvistendahl Karlsen. “ L^1 stability for entropy solutions of nonlinear degenerate parabolic convective-diffusion equations with discontinuous coefficients”. In: *Skr. K. Vidensk. Selsk.* 2 (2003), pp. 1–49.
- [31] Kenneth Hvistendahl Karlsen and John D Towers. “Convergence of a Godunov scheme for conservation laws with a discontinuous flux lacking the crossing condition”. In: *Journal of Hyperbolic Differential Equations* 14.04 (2017), pp. 671–701.
- [32] Nader El-Khatib, Paola Goatin, and Massimiliano D Rosini. “On entropy weak solutions of Hughes’ model for pedestrian motion”. In: *Zeitschrift für angewandte Mathematik und Physik* 64.2 (2013), pp. 223–251.
- [33] Stanislav N Kružkov. “First order quasilinear equations in several independent variables”. In: *Mathematics of the USSR-Sbornik* 10.2 (1970), p. 217.

- [34] S Mochon. “An analysis of the traffic on highways with changing surface conditions”. In: *Mathematical Modelling* 9.1 (1987), pp. 1–11.
- [35] David Stewart Ross. “Two new moving boundary problems for scalar conservation laws”. In: *Communications on pure and applied mathematics* 41.5 (1988), pp. 725–737.
- [36] Sylla, Abraham. “A LWR model with constraints at moving interfaces”. In: *ESAIM: M2AN* 56.3 (2022), pp. 1081–1114. DOI: [10.1051/m2an/2022030](https://doi.org/10.1051/m2an/2022030). URL: <https://doi.org/10.1051/m2an/2022030>.
- [37] John D. Towers. “A Difference Scheme for Conservation Laws with a Discontinuous Flux: The Nonconvex Case”. In: *SIAM Journal on Numerical Analysis* 39.4 (2001), pp. 1197–1218. DOI: [10.1137/S0036142900374974](https://doi.org/10.1137/S0036142900374974).
- [38] Xin Wen and Shi Jin. “Convergence of an immersed interface upwind scheme for linear advection equations with piecewise constant coefficients I: L^1 -error estimates,” in: *Journal of Computational Mathematics* 26.1 (2008), pp. 1–22.
- [39] Xiaoguang Zhong, Thomas Y. Hou, and Philippe G. LeFloch. “Computational Methods for Propagating Phase Boundaries”. In: *Journal of Computational Physics* 124.1 (1996), pp. 192–216. ISSN: 0021-9991. DOI: <https://doi.org/10.1006/jcph.1996.0053>.